Figure 4-4 shows a table detailing the effects of varying stylus angle on cell volume whilst keeping cell width and length constant. As the stylus angle is increased, the volume and cross sectional area of the cell decreases significantly, with a 140° stylus engraving a cell with only approximately half of the cross sectional area of a 110° stylus and two thirds of the volume.[15]

Stylus Angle	Volume (μm^3)
120°	81192
130°	65590
140°	51192

Assuming 150μm cell, width and length

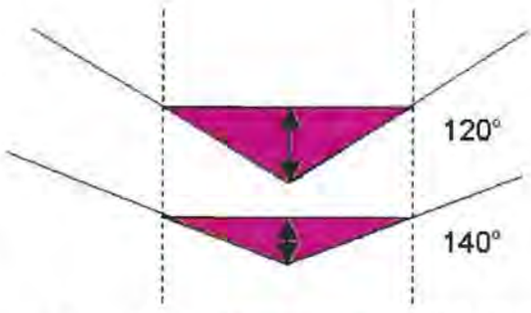

Figure 4-4 – Comparison of CSA of cells

Graph 4.26 details the effects of volume on density as stylus angle changes. Maximum density is achieved for a specified volume using a 130° stylus engraved cell. As with the results examining screen ruling, a specified volume cell will be at different points on the coverage range for different stylus angles.[16] No significant variation was observed when examining specific volume due to the number of cells/unit area being maintained as stylus angle is changed.

[15] Styli with angles as small as 90° and as large as 150° are used, with the majority of engraving work using styli between 110° and 140°.

[16] A 100% 140° cell has a similar volume to a 90% 130° cell and a 75% 120° cell.

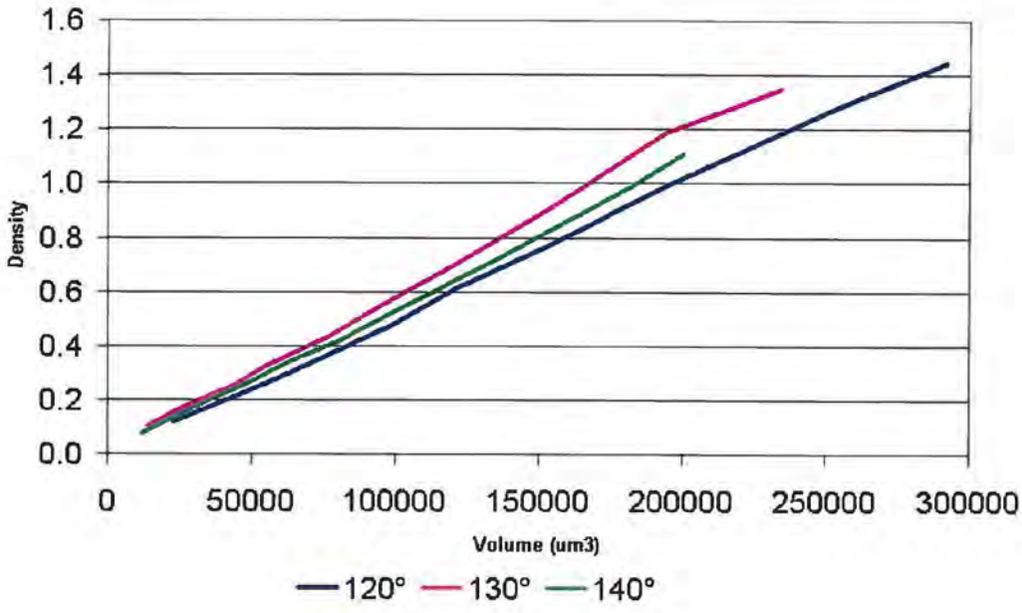

Graph 4.26 – Volume and Density

The effect of stylus angle at different coverages is shown in Graph 4.27. Volume increases significantly at each coverage level as the stylus angle is reduced.

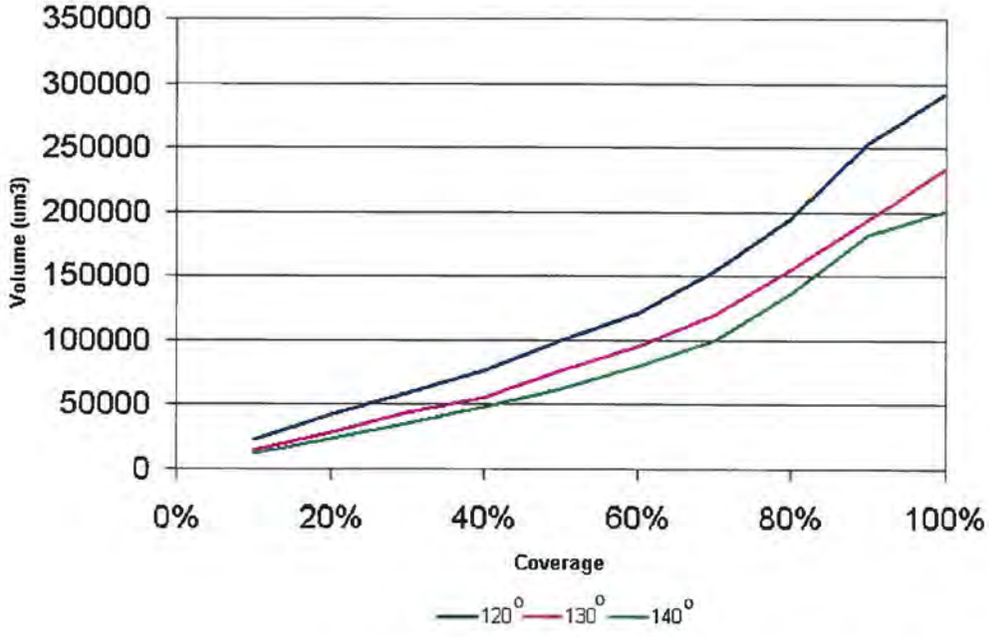

Graph 4.27 – Stylus angle effects on volume and coverage

Although volume increases as stylus angle decreases, by considering the results as shown in Graph 4.26, the solid density is not merely a function of this volume, but is also affected by the ink release process.

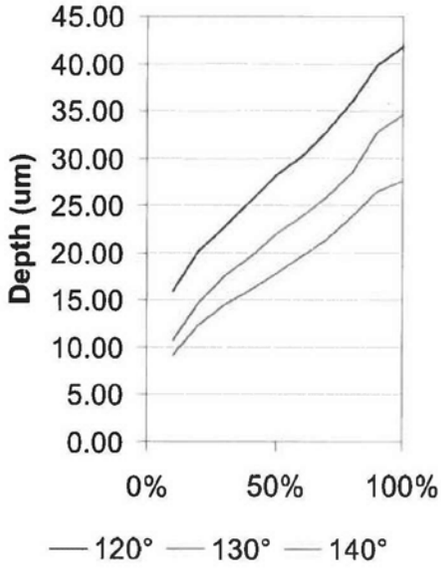

Graph 4.28a - Depth

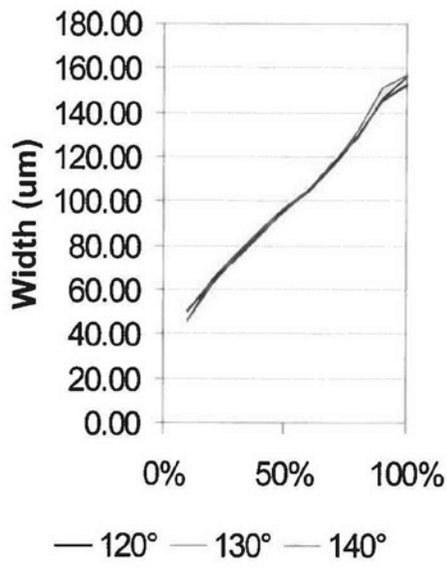

Graph 4.28b – Width

Graph 4.28 – Effects of Stylus Angle on depth and width

The effect of varying the stylus angle on the depth and width of the cells is shown in Graph 4.28. There are differences between the two sets of curves. Previously when comparing depth and width results, the effects of changing the diamonds were averaged out through the data reduction associated with the orthogonal array technique. Although three diamonds were used for the engraving, a set of cells using each diamond was measured, analysed and averaged. It is clear that by increasing the stylus angle, shallower cells are obtained, but that changing the stylus angle has not significantly altered the width of the cells.

The effects of stylus angle on length and open area are also shown in Graph 4.29. Varying the stylus angle makes no significant difference to the external dimensions of the cells being analysed, as required by the engraver.

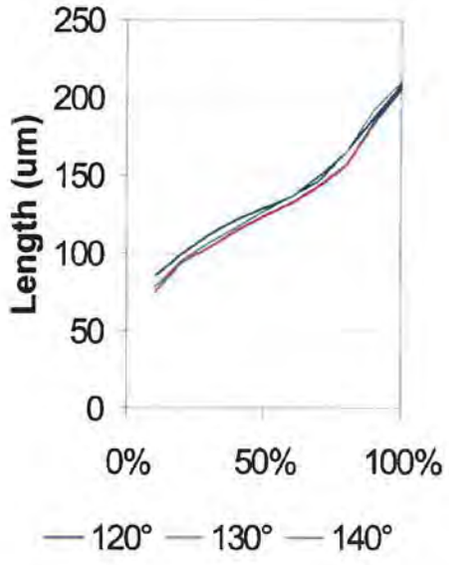

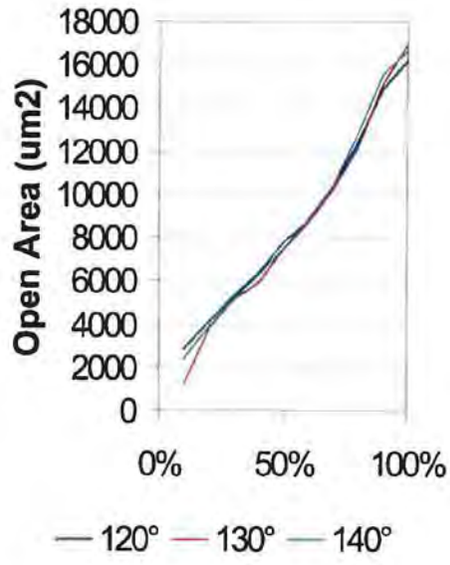

Graph 4.29a – Length

Graph 4.29b - Open Area

Graph 4.29 – Effects of stylus angle on Length and Area

Graph 4.30 details the effects of stylus angle on tone gain, compared to the tonal reproduction normalised with respect to the 130° stylus.

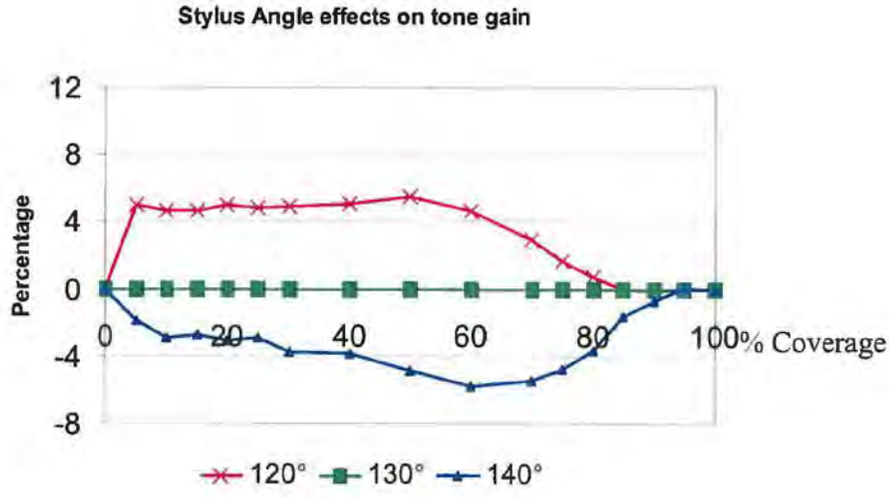

Graph 4.30 – Effects of stylus angle on tone gain

As stylus angle increases, generally tone gain decreases. This is the same finding as with the effects of screen ruling, and is also attributed to the physical dot gain. The larger printed dots spreading out more, giving near identical performance for each stylus angle. At lower coverages the tone gain decreases as stylus angle increases.

4.3.3.1 Stylus angle summary

The decrease in density with stylus angle appears to be non-linear, with the largest decrease occurring in the gap between 130° and 140° (Graph 4.25). This trend is reversed however, when comparing stylus angle with volume, where the largest difference occurs between 120° and 130°. This trend also holds with length, width and depth. Ink transfer, similarly increases (slightly) as stylus angle increases. The reasons for this apparent discrepancy are unclear. It is considered that this is due to the different release characteristics of conjoined dots (where the dots have merged together to produce a continuous layer of ink on the substrate) compared with the necessary use of individual dots observed at 30-50% coverage, as used when calculating ink release. It is believed that this is a function of the geometry of the cell

It should be noted that at stylus angle increases, the depth of the cell engraved decreases, but that the external dimensions (width, length etc) of the cells are retained. As stylus angle increases, the printed density, both solid and in the tonal regions decreases. This is due to the significantly reducing volume of the cells, making a much smaller quantity of ink available to the substrate, and thus leading to reduced printed densities.

4.3.4 Summary of geometric parameters effects

In general, as cell volume increases, printed density increases.

As screen ruling increases, printed density decreases, both in terms of solids and of tonal reproduction. This is largely due to the reduced specific volume available at higher screen rulings. As screen ruling increases, tone gain decreases. This has been

attributed to the viscosity of the ink allowing larger dots to spread out further, which was borne out by analysis of the physical dot gain of the system. It has been shown that as screen ruling is changed, the shape of the cell remains unchanged, as is the engravers intention, and that the cells are merely scaled down as screen ruling is increased.

As compression ratio increases, the depth of the cells decreases along with the width, whilst the length of the cells increases, thus approximately maintaining volume, while allowing the external shape of the cells to be changed to approximate changing the screen angle, and thus allowing the prevention of Moiré. The printed density, both solid and in tonal regions decreases as compression ratio increases, although no significant difference is observed as the compression ratio is increased from 37° - 45°. This is because the volume remains approximately constant between 37° and 45° before decreasing as the compression ratio is increased beyond 45°, despite the engravers intention to maintain volume as compression ratio is increased.

The decrease in density with stylus angle is non-linear, with the largest decrease occurring in the gap between 130° and 140°. This trend is reversed however, when comparing stylus angle with volume, where the largest difference occurs between 120° and 130°. This trend also holds with length, width and depth. Ink transfer, similarly increases (slightly) as stylus angle increases. It is likely that this is due to the different release characteristics of conjoined dots (where the dots have merged together to produce a continuous layer of ink on the substrate) compared with the necessary use of individual dots observed at 30-50% coverage, as used when calculating ink release. This is a function of the geometry of the cell. It should be noted that at stylus angle increases, the depth of the cell engraved decreases, but that the external dimensions (width, length etc) of the cells are retained, as intended by the engraver. As stylus angle increases, the printed density, both solid and in the tonal regions decreases, due to the decreased volumes

4.4 Calculation of printed dot volumes

The calculation of the volume of ink transferred to the substrate required the use of two distinct stages, the first - thermal desorption – gas chromatography – mass spectrometry (TDGCMS) and the second - white light interferometry. By knowing the volume of notionally 'dry ink', (using interferometry) and the quantity of retained solvents in the 'dry ink' (using TDGCMS), coupled with the known solvent content of the ink as supplied, it is possible to calculate the total volume of ink, which was released from the cell. This section details the results from this two stage analysis procedure.

4.4.1 TDGCMS results

The TDGCMS was used in order to ascertain the quantity of solvent in the raw substrate, the ink and the printed substrate. TDGCMS analysis is a three-stage process. Thermal desorption strips the volatile component of a sample by heating. Gas chromatography separates the volatile components from the mix supplied from the thermal desorber, and mass spectrometry identifies the components from their molecular weight and measures their abundance in the measurement sample. Although there is no literature suggesting that this technique has been used previously to precisely quantify retained solvents in printed material, the manufacturers of the equipment specify that it is suitable for this sort of testing [23] [29] [35], and similar experiments have been performed, as discussed in section 2.2.

4.4.1.1 Inks

Due to the nature of the test, it is not possible to test for methanol, and so the results from the TDGCMS were complemented by analysis of a detailed breakdown of the ink supplied by the manufacturer, and a simple dry weight analysis.

All inks were analysed, covering both colour inks used in the experiment (cyan and magenta) and both reduction techniques (conventional viscosity reduction and

constant colour strength viscosity reductions) at all viscosities. As an example, a total ion chromatogram for magenta ink, mid viscosity, using a conventional viscosity reduction is shown below, Figure 4-5.

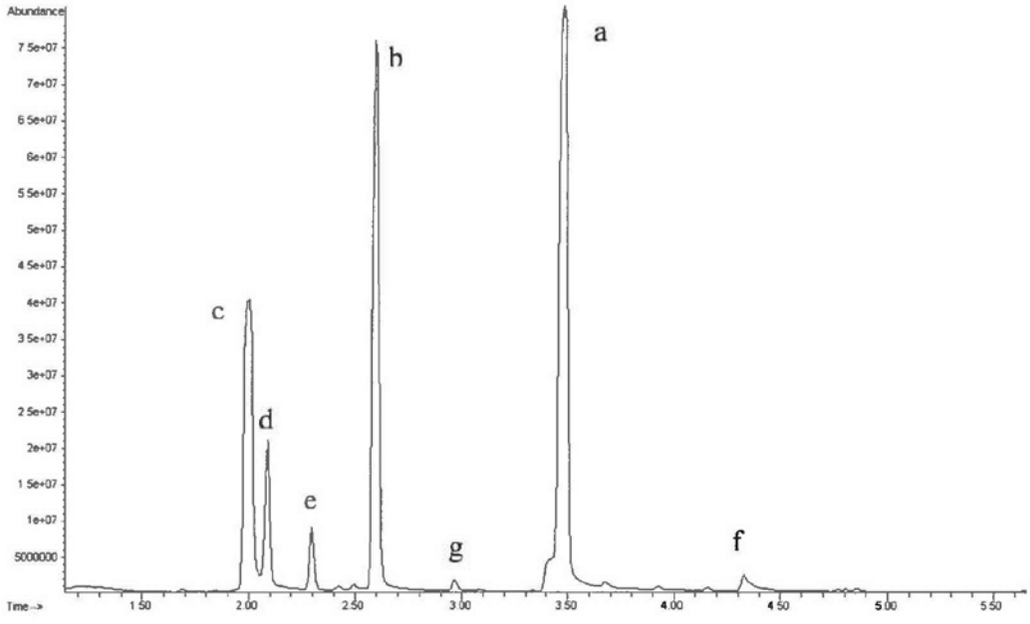

Figure 4-5 – TIC, magenta ink

Seven primary components were found in the ink. In decreasing order of significance they are :

- n-propyl acetate (NPA) (a)
- Ethyl acetate (EA) (b)
- Ethanol (c)
- Isopropyl alcohol (d)
- Propanol (e)
- 2,4-pentanedione (f)
- Acetic acid, 1-methylethyl ester (g)

Many of these are general solvents used in either the pigment, medium or 'additive'. (2,4-pentane dione for example, being used as an adhesion promoter). The breakdown of the ink supplied by the manufacturer also lists methanol as a significant component. TDGCMS however, is not capable of 'seeing' methanol (CH_3OH) as its boiling point is too low, and the sorbents inside the thermal desorber are not capable

of retaining it. As a result, the precise breakdown was used to calculate volatile content of the supplied ink. It was ascertained that the raw ink base (in each case) contained 69% ±0.5% by weight solvent. Ratios for additional solvent added (to reduce the viscosity to press-ready levels) were also supplied, the solvent levels ranging from 80% - 86% by weight.

Values for solvent content were confirmed by solid analysis. Three phials were weighed, and 1cc of ink was added to each. The ink was allowed to dry in a warm, well-ventilated place for two weeks before it was reweighed. Theoretical calculation of solids concentration indicates that there should be 0.32g of solids per cc of ink. Average solids weight measured was found to be 0.34g of solids per cc of ink. Substrate analysis was performed approximately 18 months following the trial, and solvents were still found in the prints, so it is unlikely that all the solvent has been removed from the ink – this accounts for the excess 0.02g of solids, and validates the measurements.

Acetic acid does not appear in the breakdown of the ink, and this is either contamination (for example, it occurs in small quantities in fingerprint oils) or the product of a reaction. It does however appear in sufficiently small quantities to be safely ignored without altering the results.

4.4.1.2 Substrate

Patches were measured from each ink trial, and of unprinted substrate. No significant variation in the quantities of retained solvent were observed in the results between different viscosities or reduction methods, although variation was observed between the cyan and magenta inks.

The sample size was 40x10mm. The total retained solvent/sample is listed in ng (10^{-9}g) / measurement strip. Results are shown below, in Graph 4.31 for the breakdown of cyan printed substrate, magenta printed substrate, and unprinted substrate.

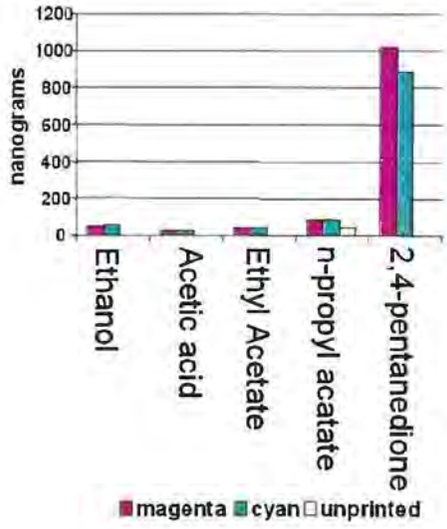

Graph 4.31 – Retained solvents in printed substrate

It was identified that n-propyl acetate occurs in both the printed and unprinted substrate. The quantities of n-propyl acetate found are small in any case, and were deducted from the solvents found in the printed substrate.

No propanol or isopropyl alcohol were observed in any samples of the prints. It is assumed therefore that these two components had fully evaporated before measurement occurred. The volume of solvent retained was calculated from the densities of the solvents observed, giving a value of 1% for retained solvent volume. Thus 1% of the total volume of dry ink on the substrate is made up of unevaporated solvents, the remaining 99% being made up from the dry components of the ink.

4.4.2 Interferometry results

Prints were examined using white light interferometry to measure the precise amount of solid ink deposited on the substrate (see 3.4.3). A film was used to eliminate penetration of the ink into the substrate. Measurements were taken at 30%, 40% and 50% coverage for reasons detailed in section 3.4.3.1. A three dimensional image of a

gravure dot is shown in Figure 4-6. A matrix showing the range of dots examined is given in Figure 4-7.

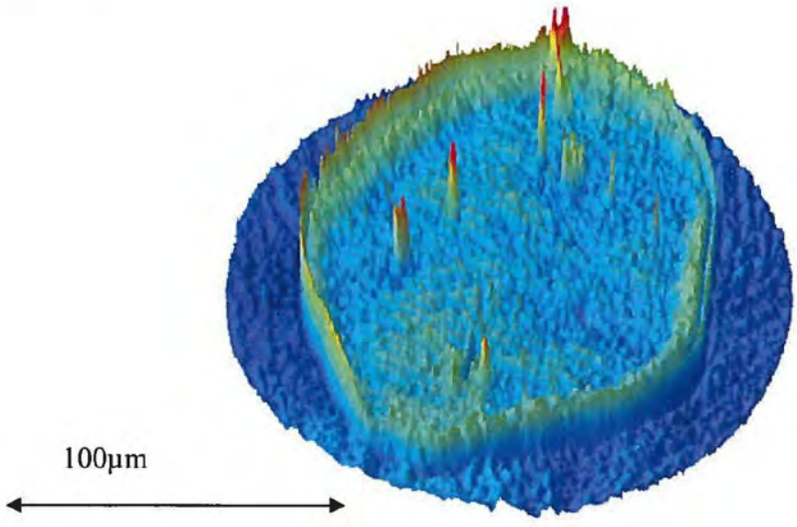

Figure 4-6 – 3D image of gravure printed dot (40% coverage, 70lpcm, 45° compression ratio, 130° stylus angle)

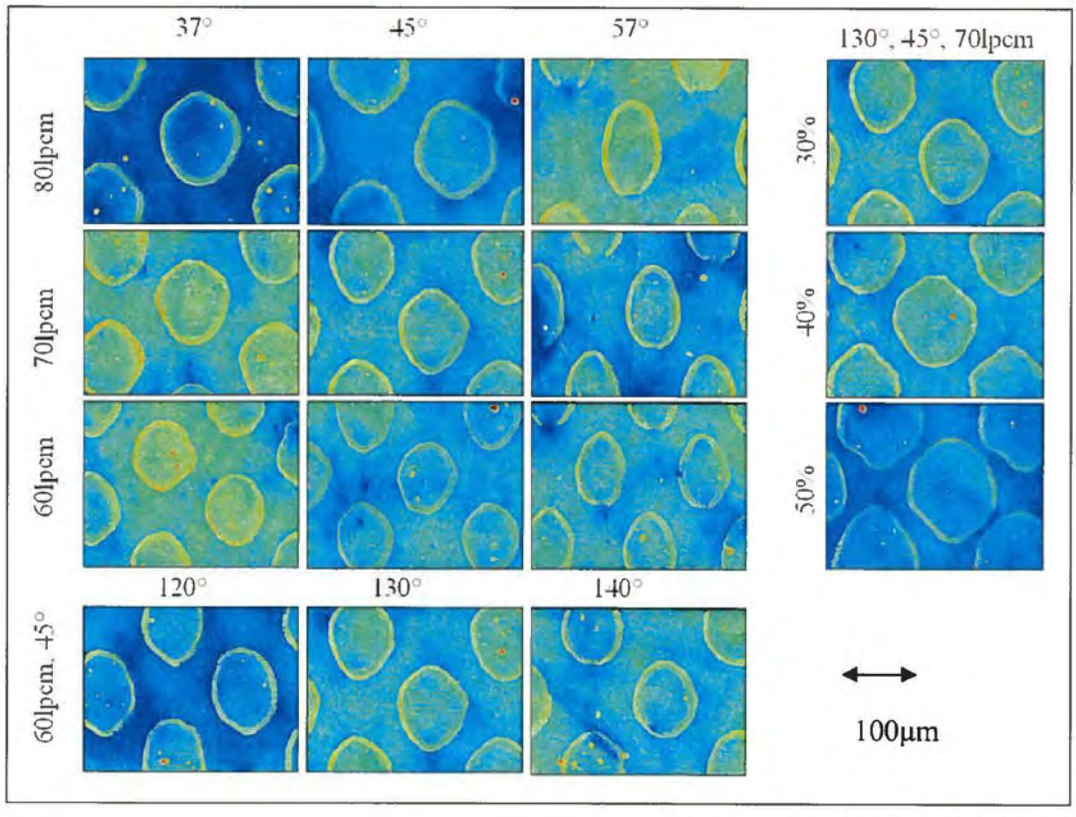

Figure 4-7 – Range of dot sizes

4.4.2.1 Optimisation of sample size

A set of measurements was taken, totalling 20 dots, from a patch. A moving average analysis was performed, indicating that measurement of 12 dots would give acceptable accuracy on the printed dot size. The calculation is as detailed in Section **3.6.**

4.4.2.2 Solid ink volumes – effects of cell characteristics

Orthogonal array techniques were used to analyse the volumes of the printed dots, analysing the way in which the dots change as screen ruling, stylus angle, compression ratio, etc are changed[17]. Histograms showing the variation of printed dot volume with compression ratio, screen ruling and stylus angle are shown in Graph 4.32. From analysis of these graphs, it can be seen that as screen ruling and stylus angle increase, printed dot volume decreases. As compression ratio increases from 37°-45°, there is a slight increase in the printed dot volume, but the printed dot volume decreases as compression ratio is increased further from 45°-57°. This correlates with the results measured for volume and open area, where there is little change in volume (albeit a slight decrease), but an increase in open area observed in the change between 37° and 45° compression ratio. It should be noted that these measured values are highly accurate and relate the release from an individual cell rather than an averaged release over a large area. As a result, this work is significantly more accurate than previous studies in the field. [25] [29] [41] [42] [43] [44] [53] [56]

[17] A worked example of this analysis is shown in appendix 3, for volume analysis of L9.1.

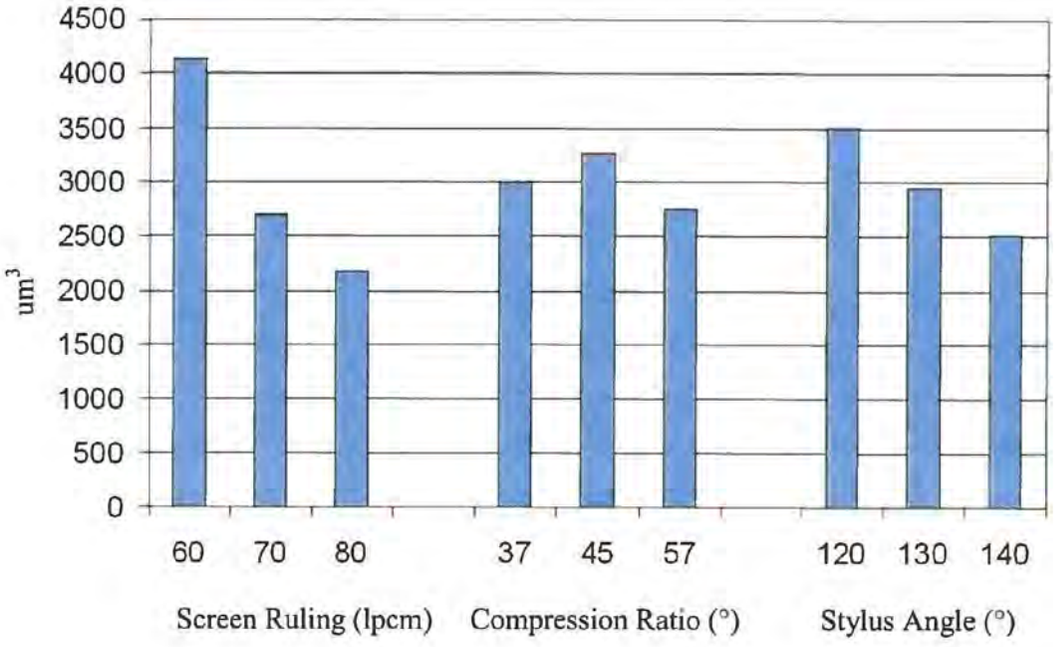

Graph 4.32 – Average dot volumes for different conditions

As detailed in section 4.2 changing the defining characteristics of the engraved cells (the screen ruling, compression ratio and stylus angle) can change the length, depth, volume etc of the cells. As a result, printed dot volumes were plotted against the various characteristics of the cells, in order to investigate correlations between them. This demonstrated that larger cells made larger dots – the entire principle of engraving. As a result of this, the data was reanalysed in terms of release.

4.4.2.3 Effects of Ink

Histograms of ink release (solid content and released volume) are given in Graph 4.33. Prints were made using inks at three different viscosities, termed high (24s, Zahn 2), medium (20s, Zahn 2) and low (17s Zahn 2). Results given are for magenta ink, using conventional reduction means (adding solvent to higher viscosity inks, lowering both the viscosity and colour strength). It can be seen from Graph 4.33a that as the viscosity increases, the volume of solid ink on the substrate increases. This is partly a transfer effect, and partly an effect caused by the dilution of the ink at lower

viscosities. Also, as viscosity rises, the total quantity of ink released from the cells also increases, with the largest changes being observed between mid and high viscosity ink. This is caused by the significant quantities of solvent required to lower the viscosity to the 17s (Zahn 2) that was required for the low viscosity trial, since by adding solvent, the surface tension of the ink is reduced, aiding adhesion, but reducing the amount of ink being pulled out of the cell, as shown in [57]. This trend was maintained with changes in coverage. Large differences were observed in the shape of the printed dots as the viscosity of the ink was changed. High viscosity ink produced dots with much sharper, well defined edges, whilst low viscosity ink spread more, providing less well defined cells. Examples of this are shown in Figure 4-8.

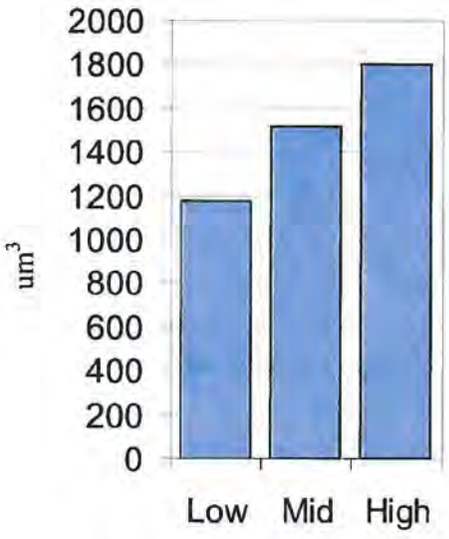

Graph 4.33a – Solid ink release

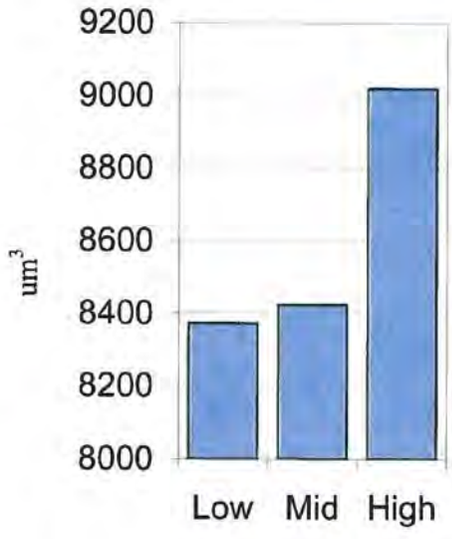

Graph 4.33b – Total ink released

Graph 4.33 – Ink release with viscosity

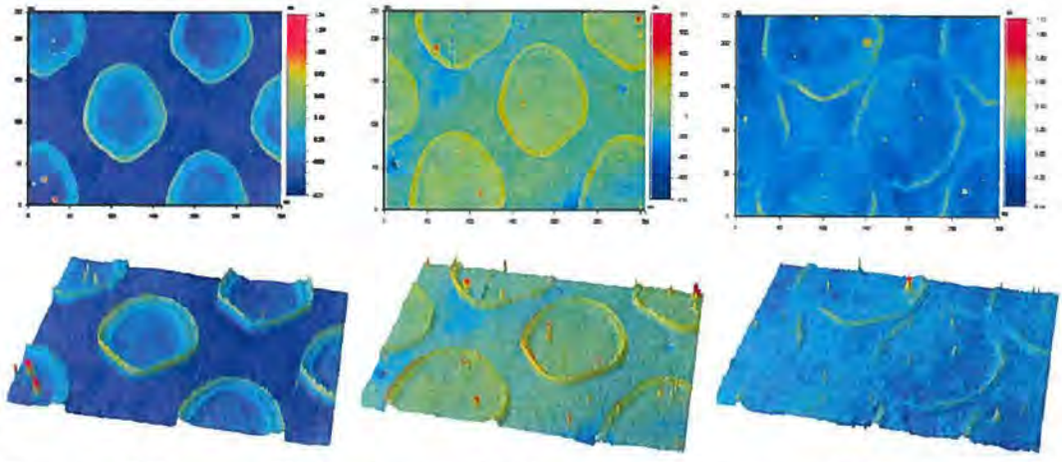

Figure 4-8a – High viscosity

Figure 4-8b – Mid Viscosity

Figure 4-8c – Low viscosity

Figure 4-8 – Different viscosity dots (50% coverage, 70lpcm, 45° Compression ratio, 130° stylus angle)

This is likely to be caused by the slumping mechanisms of the drying ink. As the low viscosity ink has a higher quantity of solvent related to each individual dot, the drying time of that dot will be higher than the drying time of a higher viscosity dot, which has a lower amount of solvent associated with it. As a result, this extended drying time has led to the low viscosity ink dots spreading further.

4.4.2.4 Discussion of errors in dot volumes

As detailed in section 3.6, the random variation in dot sizes is significant, and relatively large numbers of dots needed to be measured in order to have confidence in the measurements. Appendix 6 details the variation in dot sizes, and demonstrates that size variations of the level observed are caused by process variation with 99.999% confidence.

4.4.2.5 Dot volumes and printed density

The printed dot volumes of all dots, from all available coverages (30-50%), 60, 70 and 80lpcm screen rulings, 37°, 45° and 57° compression ratios and 120°, 130° and 140° stylus angles, as taken from the orthogonal array matrix were also plotted against density (Graph 4.34). An increase in printed dot volume leads to an increase in printed density, although the correlation band is not particularly close.

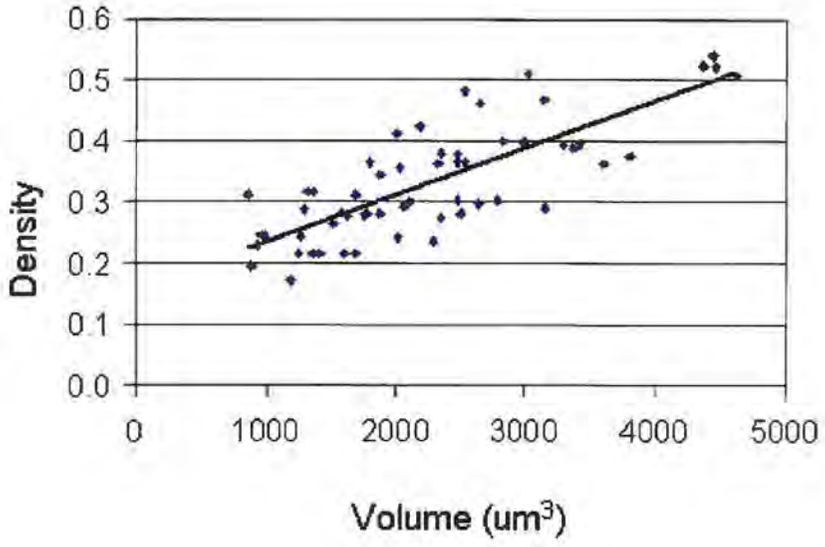

Graph 4.34 – Printed dot volume and density. (30-50% coverage, all screen rulings, all stylus angles, all compression ratios. Magenta ink, conventional reductions)

Density is a measure of the reflectance of the sample, and as such an increase in transferred volume would be expected to lead to a decrease in reflectance, and thus an increase in density. This can be seen generally, although it would be expected for data to fit more closely to the correlation. The lack of a simple, clear line indicates that something other than volume is important in producing the printed density. This is largely due to the spreading effects of the ink. Under certain conditions, for example, with lower viscosity inks, as identified in 4.4.2.3,the ink spreads out more, providing a larger, thinner ink covering. These in turn lead to an increase in the printed density.

The volumes of dots are also skewed by the presence of entrained particles, which do not significantly affect the printed density.

4.4.2.6 Total released volume

Total released volume is the sum total of the printed dot volume (the solids remaining after solvent evaporation), and the solvents evaporated from that quantity of solids. The TDGCMS experiments indicated the presence of 1% (volume) of solvents remaining in the solid ink, and that the raw printing ink was made up of 80%-86% solvent, depending on the ink in use (82% for magenta ink at mid viscosity). From this it was established that the total volume of ink released (for mid viscosity, conventional reduction ink) could be calculated from:

$$0.99 \times (\text{Printed dot volume}) / 0.18 = \text{Total released volume}$$

Equation 4.2 – Ink release calculation

As shown in section 4.3, printed density on tonal reproduction is affected by screen ruling, stylus angle and compression ratio. Thus the volume of ink released is likely to be affected in a similar manner.

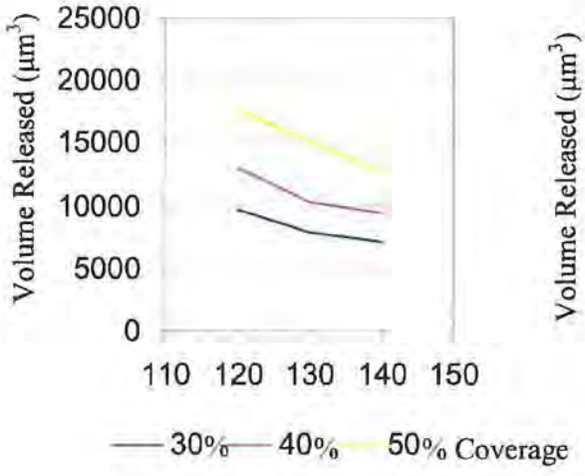

Graph 4.35a – Stylus angle (°)

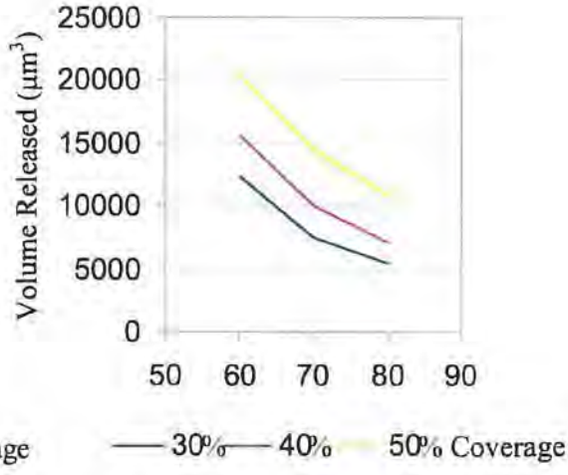

Graph 4.35b – Screen ruling (lpcm)

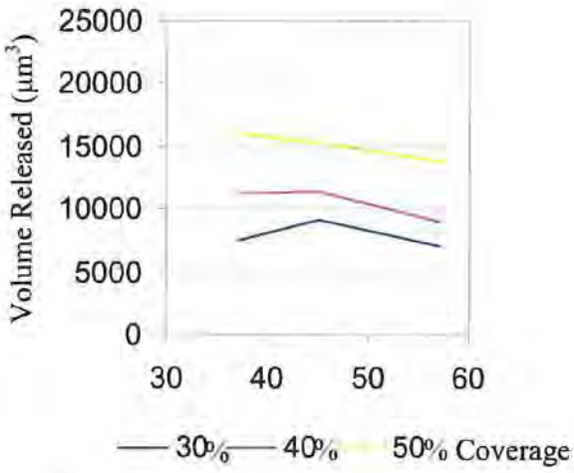

Graph 4.35c - Compression ratio (°)

Graph 4.35 – Effects of variables on release

In each case, the trends regarding the total volume of ink release correlate with the measurements of cell volume in section 4.2. A larger cell contains a larger quantity of ink and thus more of it is available to be released. Hence the higher release volumes observed with the larger cells engraved at lower screen rulings, stylus angles and (generally) compression ratios.

4.5 Calculation of ink release ratio

This section is one of the focal points of this work. Other investigators have used a variety of techniques to investigate the proportion of ink released from gravure cells, but their methods have been limited by the measurement techniques that were available at the time. In each experimental work the cell volume has been theoretically calculated. This, as shown in section 4.2 significantly underestimates the cell volume compared to those which have been measured using interferometry. In addition, the analysis techniques used involve averaging over large areas, rather than investigating the release from individual cells. Furthermore, the accuracy of the averaging techniques for films of the thickness under investigation is in question. As a result, this work provides the first, accurately quantified value for ink release from

gravure cells, utilising highly accurate cell volume measurements and highly accurate dot volume measurements. The latter also accounts for retained solvent quantities and an accurate breakdown of the ink to produce these values.

As demonstrated in 4.4.2.6 the total volume of ink released from a given cell has been calculated. The volume of a cell was measured and calculated in section 3.2.5.

As discussed in section 2.3.1, previous work performed by Kunz [25] has indicated that the cells are not completely full after doctoring, and that some ink is removed by the doctoring process. No method is readily available to quantify the filling state of the cells, particularly when using production inks. Kunz [25] gives cross sections of cells indicating the filling state at various times after doctoring. From analysis of these diagrams, a filling state of 95% is indicated. This was calculated using an early interferometric technique identifying a meniscus in the fluid surface within the cell, and although the trial was performed using unrealistic inks it is reasonable to assume that a small amount of the ink is 'scraped out' by the doctoring process.

The percentage ink release was thus calculated for each of the conditions to examine the effects of the different variables. The results account for the filling state [25] and they are shown in Graph 4.36. A relatively wide spread of results are observed due to the large number of conditions being examined with the orthogonal array matrices. However, a simple linear regression trendline was plotted to indicate how the data changes with respect to the screen ruling, stylus angle and compression ratio.

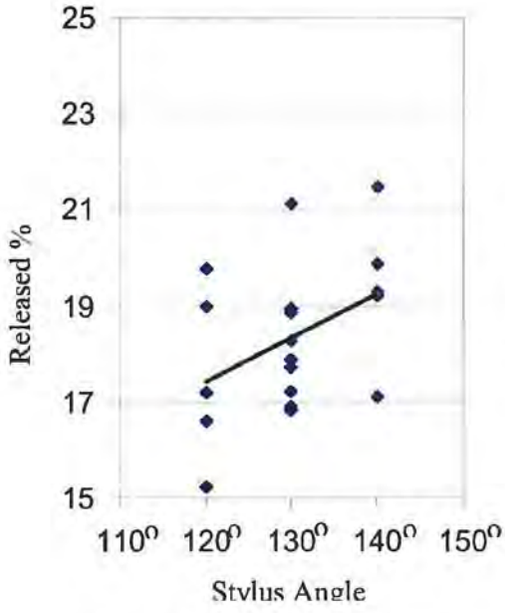

Graph 4.36a – Effects of stylus angle

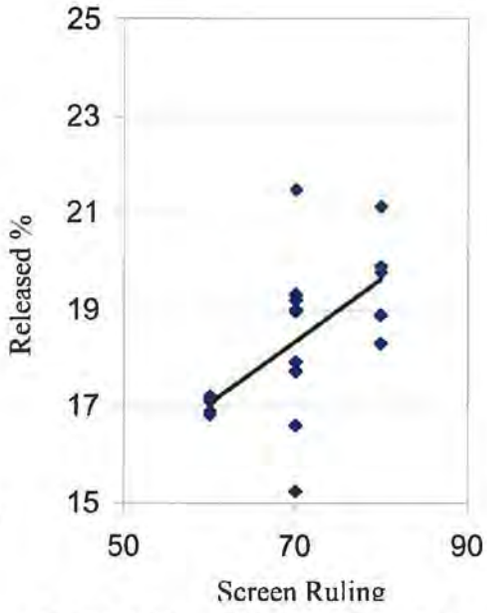

Graph 4.36b – Effects of Screen ruling

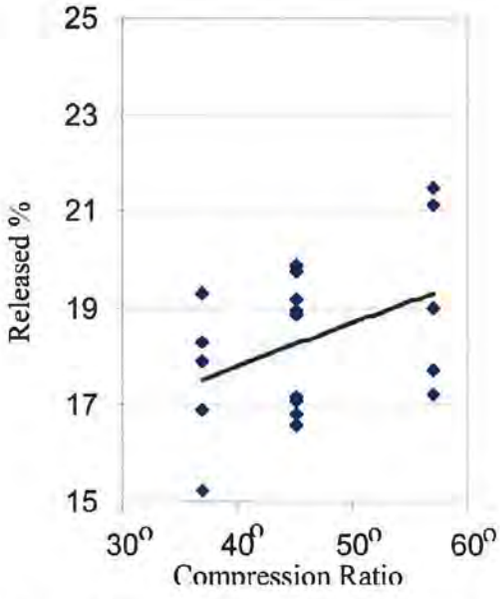

Graph 4.36c – Effects of compression ratio

Graph 4.36 – Percentage release from cells

Most dramatically, it can be seen that the percentage release of ink from cells is typically approximately 18%. The release is also affected to some extent by stylus angle, screen ruling and compression ratio.

These values are all significantly lower than most previously published results, both theoretical and practical [25] [29] [41] [42] [43] [51] [52] [53], although they are comparable to the work of Kapur, Gaskell and Bates [54] and Benkreira and Cohu [52] who calculated release at between 15% and 20%.

It is widely held in the gravure industry, that the release of ink from cells is significantly higher than that observed in this study. It has been suggested that the low figures for ink release presented here are as a result of significant evaporation occurring between doctoring and the printing nip.

Evaporation is a function of many different variables, including temperature, air/surface interfacial speed, humidity, vapour and partial pressures, volatility etc. Stefan's law (Equation 4.3) defines evaporation in terms of diffusion, where;

$$m_w = \frac{DpMA}{R_0 T.\Delta X}.\ln\frac{(p - p_{a2})}{(p - p_{a1})}$$

Equation 4.3 – Stefan's law

As a first approximation, given that the solvent used is made up of many different components, considering for the most volatile component (Methanol – CH_3OH) will give a 'worst case' scenario for evaporation – calculated to be at the rate of 6g of methanol/hr. It is assumed that a layer of 1um of ink is passed under the blade for lubrication. 6g/hr equates to a loss of 1.6mg/s or 2 x 10^{-3} cc/s. The time delay between doctoring and printing is approximately 60ms, thus the total solvent evaporated between the blade and the nip is equal to 0.13 x 10^{-3} cc – or a total of 0.4% of the available ink. Considering that this is a 'worst case' scenario, the actual evaporation will be lower than this, and thus evaporation is not a significant source of error in the release calculations.

In order to explore the impact of cell geometry on the ink release process, results were calculated to investigate the effect of changing cell length, depth and open area and

these results are presented in Graph 4.37, with linear regressions imposed to identify trends.

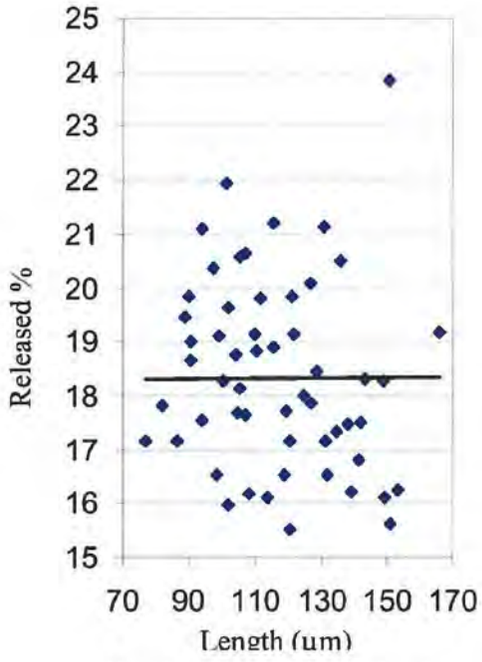

Graph 4.37a – Length (μm)

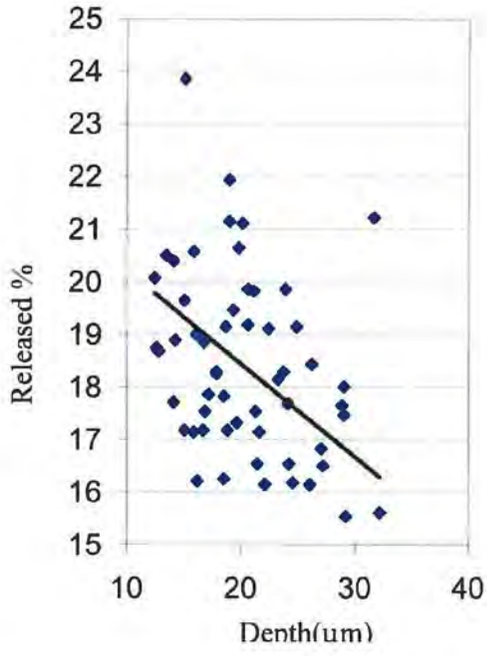

Graph 4.37b – Depth (μm)

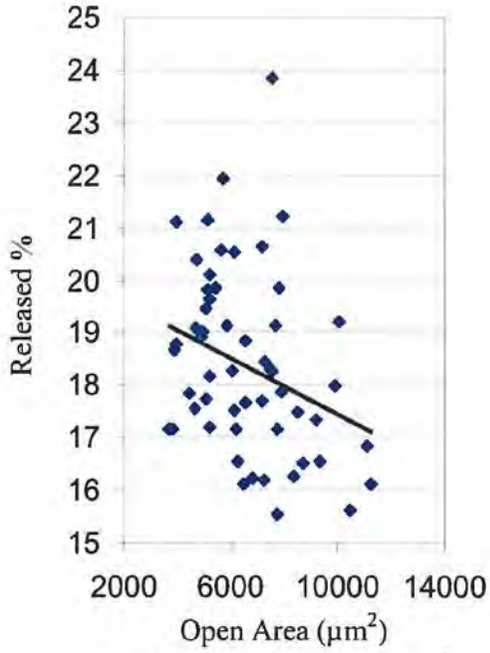

Graph 4.37c - Open area (μm^2)

Graph 4.37 – Cylinder parameter effects on ink release

In each case, the trends observed are indicative of the way in which these variables will affect the ink release behaviour.

The cell length has no significant effect on the release characteristics of that cell. However, as compression ratio increases, the ink release increases. As the effect of increasing the compression ratio is to decrease the depth/width of the cells and to increase their length, a closer correlation was expected. As compression ratio decreases, the depth of cells increases in line with the width, in order to compensate for the reduced length of the cells. As depth increases, release decreases, and also that as compression ratio decreases, release decreases. The same trends were observed between open area and screen ruling.

As cells get deeper, the release of ink from that cell drops (Graph 4.37b). This is inconsistent with previous theoretical work, which suggests that larger cells should allow more ink to be released. Kunz however demonstrates that cells with pointed bases retain more ink than those with rounded bases. As a deeper cell will lead to a more pointed base, it therefore follows that a deeper cell should retain more ink. It can also be seen in Graph 4.37c that as the open area of a cell increases, the release from that cell decreases. Schwartz [56] suggests that this may be due to refilling of the cell due to ink being squeezed out of the cell under impression. Kunz also suggests that this may be due to flow within the cell.

Benkreira and Patel [55] observed in models of ink transfer from several different types of cell, that release was independent of cell shape at approximately 30% of cell volume. They also observed that at lower Reynolds numbers (Equation 4.4) the ink transfer increases, but that under normal operating conditions the release is equal to 1/3 specific cell volume.

$$\mathrm{Re} = \frac{\rho u_s}{\mu} \cdot \frac{v_c}{a_c}$$

Equation 4.4 – Reynolds number

Given that Reynolds number decreases as viscosity increases, this would explain the increase in release for the high viscosity ink. This also agrees with the views of Powell, Savage and Guthrie [57].

Benkreira and Patel [42] and Benkreira, Patel, Naheem and LeClerq [43] have both calculated release as approximately 33%. Since the volume for the cells engraved to their specification will be approximately 20% larger than the volumes used in their calculation, and they state that release is proportional to volume, it is reasonable to assume that in reality the release from the cell sizes calculated are going to be 20% lower than calculated, or approximately 26% release. Given the errors in calculation these figures are very close to the 18-20% release figures calculated here, the errors in the measurement techniques used being significant, and which could easily lead to errors of the order of magnitude observed between these measurements and the other experimenters work. If the effect of channels is negated, as is the case with Benkreira's work, the error increases, and the cell volume is approximately 30% larger than that used for calculation. As a result, the results become extremely close, and the validity of the previous work is demonstrated, and the problems inherent with the calculation of volume from image analysis techniques is also demonstrated, this having caused the variation observed between the old and new work.

Finally, correlations are also drawn to the work performed by Powell, Savage and Guthrie [57]. It is suggested in [57] that if volume is maintained and that cell depth is increased, release will decrease due to the significantly increased adhesion between the ink and the cell walls. This is also shown (to a lesser degree) with the change in stylus angle, Graph 4.36. No change is observed with change in length as if the length is increased, the width must be decreased to maintain the same volume, and thus although the slope of one side has been increased, the slope of the other side has decreased, thus negating the effect of changing the first slope.

4.6 Closure

In this chapter, the effects of varying engraving conditions have been examined, in terms of the printed density and the physical characteristics of the engraved cells. Their effect on the release of ink from the cells has been examined and calculated from analysis using interferometry to calculate the volume of dry ink transferred and thermal-desorption-gas-chromatography-mass-spectrometry to calculate the quantity of volatile solvent remaining in this ink layer, along with a detailed breakdown of the ink supplied for the trial to calculate the quantity of ink in the original ink mix. This ink release has been identified as approximately 18% ±3%, which is comparable with the work of Benkreira and Cohu [52] and Kapur, Gaskell and Bates [54].

Although the precise release values disagree significantly with the release percentages calculated by Benkreira and Patel [55] and Powell, Savage and Guthrie [57] the trends which they have observed relating higher viscosities to higher release values have been shown here to reflect to some extent practical application.

Chapter 5

Results and Discussion

Ink Release from Non-Image Areas

5.1 Introduction

Ink release from the non-image parts of gravure cylinders is a significant problem in the gravure industry, where it is known as 'scumming' or 'hazing'. This chapter describes in detail, the measurement and analysis of the cylinders and prints made. The purpose of this study was to quantify the ink release from the non-image parts of the gravure cylinder, and to understand the fundamental mechanisms driving this transfer and thus how to begin to solve the problem of scumming.

The chapter is divided into four primary sections. The first examines the details of the cylinder, and quantifies how the surface finishes compare both in terms of the surface topography, and in terms of the effect that this has on the level of scumming. The second section investigates the effect of varying the blade load on the level of scumming. The third examines the effects of ink viscosity and type, whilst the final part examines the effect of changing the substrate.

Significant interactions have been observed between the ink, the surface finish, the doctor blade, and the substrate with each affecting the response of the others, however, the results are presented so as to enable discussion of these effects separately.

5.2 Existing theory

Despite the significance of scumming as a problem in the gravure industry, little work has been performed to explore the mechanisms that are present. There are two junctions of specific interest, the junction between the gravure cylinder and the doctor

blade, and the junction between the gravure cylinder and the substrate. Since scumming reflects the transfer of a film downstream from the doctor blade nip, this suggests that the root cause is the inability of the blade to clean ink completely off the non-image area of the cylinder. This implies that scumming may be minimised through exploring the interaction with the doctor blade, or through minimising transfer of thin films at the cylinder substrate junction. Generally the current work focuses on the blade-cylinder nip, however the development of low scum inks may be more important with respect to transfer at the cylinder substrate junction.

The cylinder – blade junction can be considered to be a lubricated contact and that thin film hydrodynamics govern the interaction. Generally the behaviour in a lubricated junction can be characterised using a Stribeck Curve, as shown in Figure 5-1. This defines three regimes, hydrodynamic, mixed and boundary lubrication. Due to the extremely high stresses that occur at the tip of the doctor blade, coupled with the low ink viscosity, it is likely that the interaction at the blade tip is described by boundary layer interaction, especially at higher blade loads.

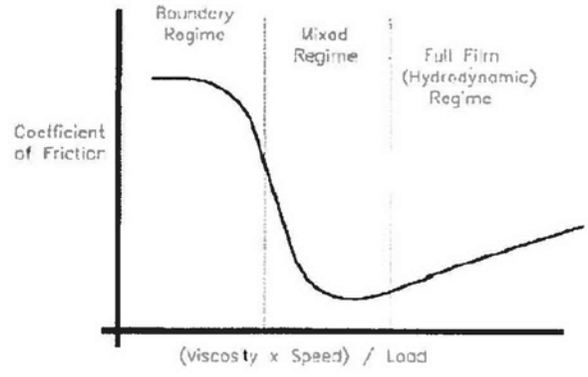

Figure 5-1 – The Stribeck curve

This behaviour at the doctor blade nip is further complicated by the flexible nature of the blade itself. For this reason, as mentioned in section 2.3.4.1, a model specific to this application has been proposed in the literature based on coating and this is shown in Figure 5-2. The mechanisms that are present again cover hydrodynamic to boundary layer lubrication regimes. Information is presented in terms of film thickness and load, since these are of most direct relevance. The film thickness infers

the quantity of fluid that passes under the blade and load adjustment is the primary method of control in doctoring. With regard to scumming, the graph implies an optimum, defined by point 'B' on the curve.

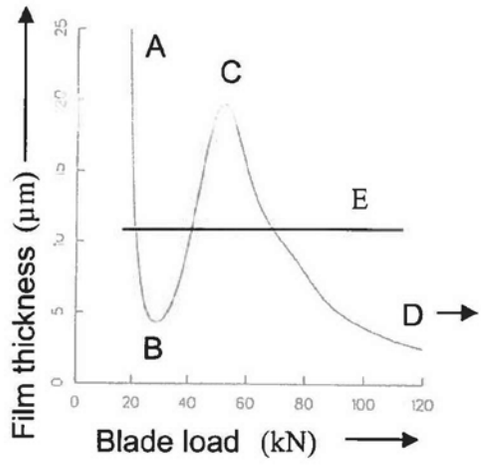

Figure 5-2 – Blade coating response (From Kistler and Schweizer [23])

The behaviour characterised by the graph may be explained as follows. As the blade is brought closer to the substrate surface, the blade initially remains straight, reducing the film thickness (moving from 'A' to 'B' in Figure 5-2). However, as the blade is brought closer, the hydrodynamic forces under the blade increase, forcing the blade to bend (point 'B'). At this point the tip of the blade moves away from the surface, allowing a thicker film to be laid down, despite the increase in blade load being applied. A further load application causes a local maximum in film thickness (point 'C')and even further increase of the blade load brings the bent blade closer to the surface, reducing again the thickness of the applied film (point 'D' onwards). It also indicates that small adjustments to the blade load may increase the film thickness passing under the blade (moving from 'B' to 'C'), decrease the thickness (moving from 'A' to 'B') or make little difference. Also, the line on Figure 5-2, indicated 'E' crosses the curve at three points. Where the line crosses the curve, the same film thickness will be pass under the blade, despite the line crossing at three significantly different blade loading conditions.

This work will explore the application of the characteristic shown in Figure 5-2 to provide insight into the mechanisms of scumming. It is likely that the factors that were changed in the experiment will affect the form of this characteristic and this will be presented and discussed in the following sections that will address surface finish, blade load, substrate and inks.

5.3 Effect of surface finishes

Cylinders were produced with several different surface finish characteristics per cylinder. The polishing of both the copper and chrome surfaces was varied using polishing stones and papers of different grits/grades, or in certain cases by not polishing the surface after milling on the polishmaster. These cylinders were then printed using different inks and substrates to investigate how each surface finish performed under production conditions, and using production materials. For details of the finishes and operating conditions, see section 3.2.2.2, and 3.3.2. The surfaces finishes are shown in Figure 5-3.

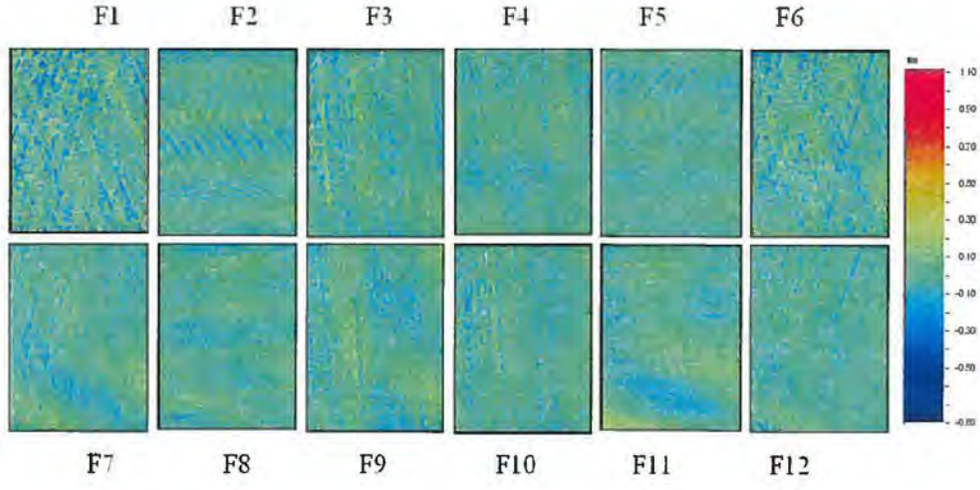

Figure 5-3 – Matrix of surface finishes[18]. Polished chrome surface, just before printing. Cylinders 1 and 2

[18] All finishes forced to the same scale (shown) so that roughness may be visually compared. Surfaces are not shown for cylinder 3, as they are repeats of ones used in F1-12. F13 is identical to F12, F14 and F15 to F4 and F16 to F6.

5.3.1 Evolution of surface finish

Sixteen surface finishes were produced on three cylinders, and run over two trials. The cylinders were prepared to several different specifications, ranging from a mirror-smooth surface (R_a = 50nm) through to rough (R_a = 300nm). Surface finish measurements were taken following copper preparation, engraving, chroming, finishing and printing (for 45s, producing approximately 200m of print), allowing the evolution of the surface finishes to be plotted. Graph 5.1 shows the evolution of the surface finish of cylinders 1 and 2, in terms of the R_a value of the cylinder, investigating how the surface characteristics change as the cylinder is engraved, chromed, polished and printed.[19] Finishes are also shown in Figure 5-3, where the extremely rough surfaces (F1, F6) are clearly seen to be the roughest surfaces.

Note on graph :

Cu – pre = Copper, before engraving
Cu – post = Copper, post engraving
Cr – pre = Chrome, pre finishing
Cr – post = Chrome, post finishing
Cr – print = Chrome, post printing

[19] R_a is used here as indicative. Several other parameters were considered, including R_z, R_q, R_t, R_z, R_{ku} (kurtosis) and R_{sk} (Skew). The four 'normal' roughness parameters (R_a, R_z, R_q, R_t) all showed the same trends, as detailed in Graph 5.1. Kurtosis and Skew failed to show any clear trends. Thus R_a is used for simplicity and clarity as it is well understood within industry.

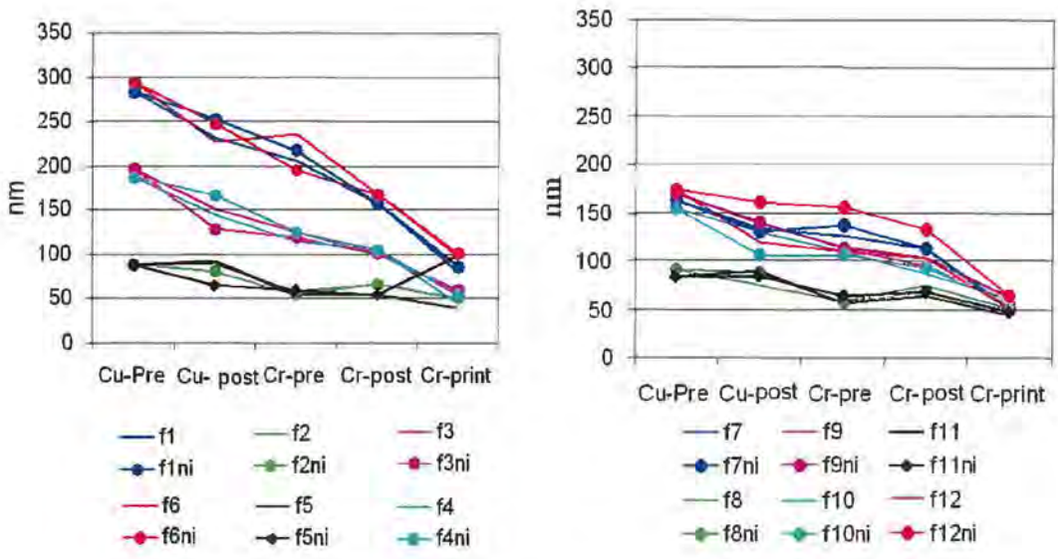

Graph 5.1 – Evolution of surface finish – Ra, first two cylinders (Finishes f1-f12 are detailed in section 3.2.2.2)

The engraving process decreases the surface roughness of most of the surfaces in both image and non-image regions, with only one of the two 'polishmaster only' finishes increasing in roughness. This is largely related to the action of the reference diamond, which is dragged along the surface of the cylinder, removing the larger protrusions from the surface. The increase in roughness of the polishmaster finish, and the relatively small decrease of the other polishmaster finish, relative to the other four finishes is due to the extremely smooth nature of these finishes, which have a minimal number of protrusions, and therefore has actually been slightly damaged by the action of the reference diamond passing by.

Little change occurs to the surface as it is chromed, with small decreases observed in almost all surface finish conditions. This is due to the chrome 'filling in' the smaller cavities, and leaving a smoother surface. On polishing however (where conventionally, it is believed that the surface roughness is increased) a significant decrease in the surface roughness is observed. This is caused by the action of the emery paper / polishing stone removing the local high areas of the surface. It is believed that this is repeated when the press operators further polish the cylinder to attempt to prevent scumming occurring.

Following printing, a further decrease in the surface roughness was observed, bringing all surface finishes relatively close in terms of overall surface roughness. One increase of surface roughness was observed, in the non-image region of finish 5. This is due to significant damage to the cylinder surface, caused by the smoothness of the initial finish. The absence of ink on the surface has eliminated lubrication with the doctor blade, which has significantly worn the surface of the cylinder, damaging it, leading to high levels of scumming on the substrate. This is shown in Figure 5-4 and Figure 5-5, below, which shows the surface of the cylinder after printing, in the image and non image regions.

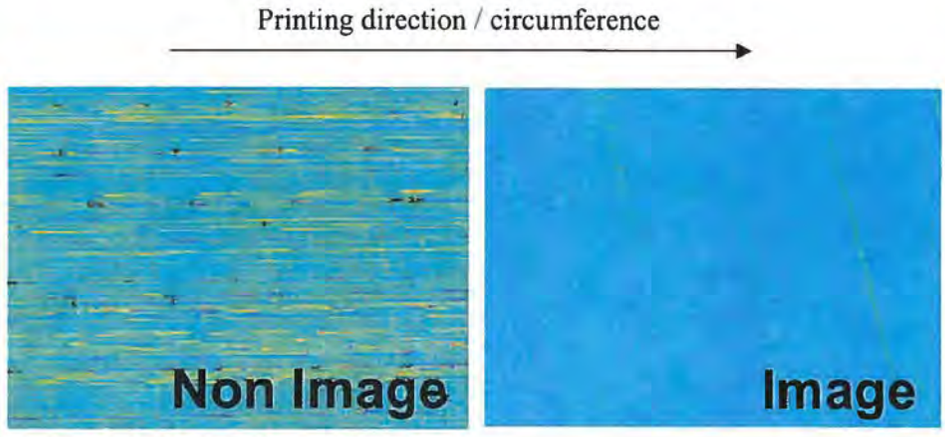

Figure 5-4 – Cylinder surface finish after printing – image[20]

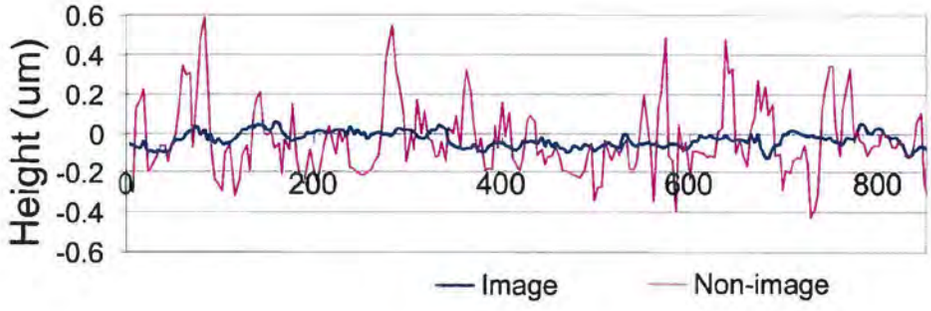

Figure 5-5 – Surface height after printing - trace

[20] The diagonal lines visible on the image section are from the 'polishmaster' machine. They are a function of the milling process.

The non image area part of the surface, which should be completely clear of ink, all around the circumference, has been badly damaged by the action of the doctor blade. This is due to the lack of lubrication supplied by ink carried on the extremely smooth surface.

These trends are repeated on the other two cylinders, and in terms of Rq, Rz, Rt, etc, Rq and Rz for cylinder 2 are shown in Graph 5.2.

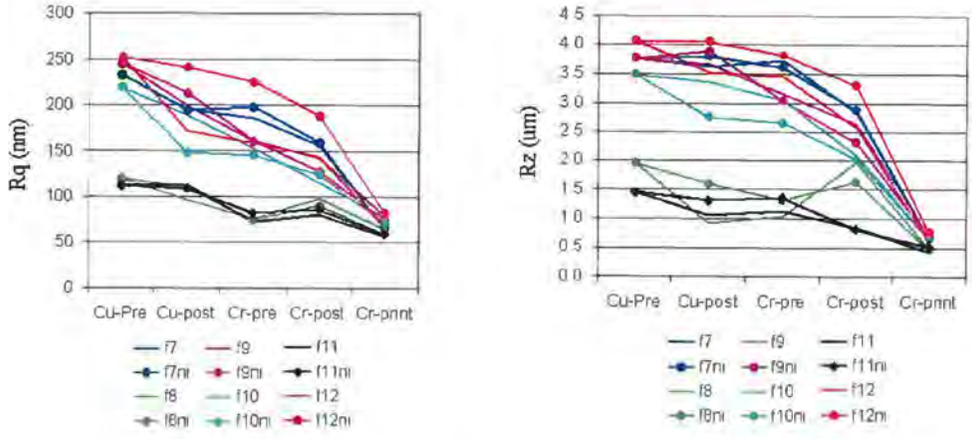

Graph 5.2 - Roughness evolution (Rq and Rz, cylinder 2)

If scumming occurs on a job, it generally occurs at the beginning of the job. As a result It is widely believed that scumming occurs when the surface finish of the cylinders is too smooth, keeping the doctor blade closely in contact with the cylinder, and preventing ink from passing underneath the blade, lubricating it. To this end, when scumming occurs, many printers will immediately polish the cylinder with a piece of emery cloth, in an attempt to 'rough up' the surface [9] [13] [63] [64] [65] [66]. It can be clearly seen from analysis of Graph 5.1 and Graph 5.2 that on polishing, the surface is actually smoothed, thus the required result is being achieved but for wrongly perceived reasons.

5.3.2 Effect of surface finish

The effects of surface finish on scumming level are shown in Graph 5.3, where surface roughness is plotted against the scumming level, expressed as the colour difference (ΔE) between the printed and unprinted substrate in the non-image regions on a clear OPP film. Thus the ΔE value just exceeds 1.0 and this change will not be readily perceptible. On first analysis, there appears to be a slight correlation between the levels of scumming observed and the surface finish of the cylinder, Graph 5.3a, where higher roughness values tend to lead to higher scumming levels. However, if the data for the extremely high roughness finishes is removed (as they are not practically relevant), it is seen (Graph 5.3b) that there is no direct correlation between the surface roughness, and the levels of scumming observed on the finished prints for this film, as the scumming levels caused by a finish with approximately 50nm Ra ('F5' in Graph 5.3b) and a finish with approximately 100nm Ra ('F4' in Graph 5.3b) are almost identical, while the points 'F2' and 'F3' are also significantly different in Ra, but similar in scumming level.

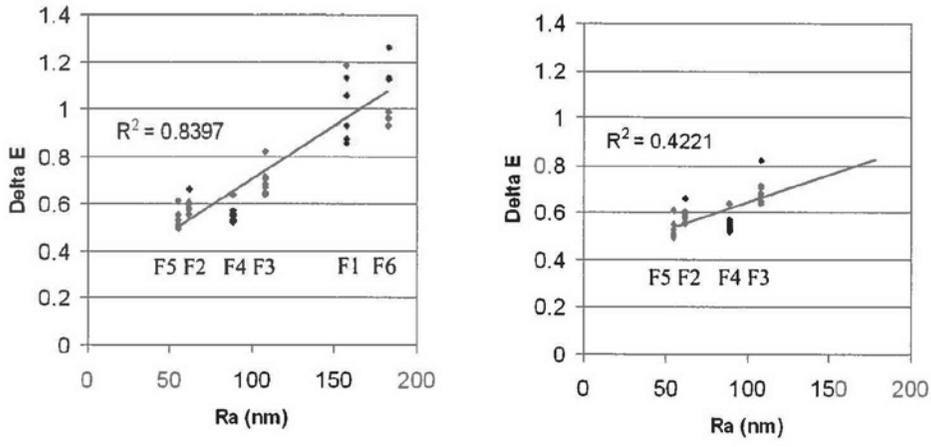

Graph 5.3 – Roughness (R_a) and Delta E (scumming level) for Clear OPP, cylinder 1, black PVB ink, all blade loads[21]

[21] For clarity Graph 5.3 uses results taken from clear films. This film exhibited lower scumming overall, but shows the effects of surface finish more clearly between F2, F3, F4 and F5.

Tests were also carried out using a white OPP substrate and the results are shown in Graph 5.4. Here, the ΔE value is significant and easily perceived visually (maximum ΔE of approximately 10) .

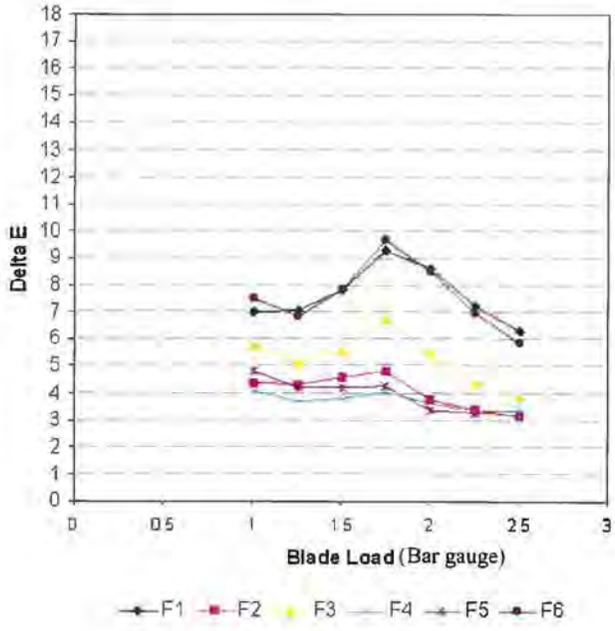

Graph 5.4 – Colour difference evolution with blade load, cylinder 1, White OPP, black PVB ink

It can be clearly seen here that F1 and F6 (the two surfaces with copper polished with paper) exhibit significantly higher scumming than the other surfaces. F3 also shows elevated scumming levels when compared with the other three surfaces. The chrome on F3 was also polished with paper. The other three surfaces, despite significant differences in their roughness (R_a values) exhibit approximately the same levels of scumming. This points to the existence of an operating window, wherein the surface finish does not significantly affect scumming unless grossly rough finishes are used. Under normal conditions, most engraved surface finishes should come within this window and thus should not cause significant amounts of scumming.

The results for cylinder 2 are presented in Graph 5.5. This shows a slightly different trend. Here, a finer paper was used for copper polishing (9μm, rather than 15μm). This has led to surfaces not being clearly distinguishable by copper polishing type. Here, the surfaces are separable by chrome finishing type.

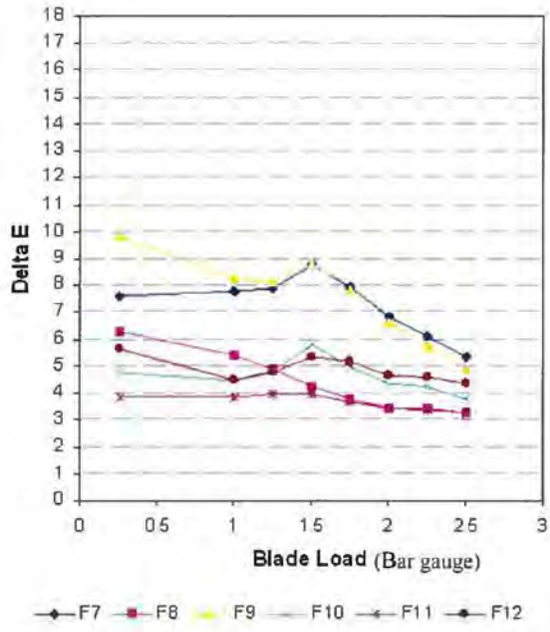

Graph 5.5 - Colour difference evolution with blade load, cylinder 2, White OPP, black PVB ink

It can be clearly seen that F7 and F9 (9µm paper and 3000grit stone, respectively in copper, 15µm polishing in chrome) exhibit higher levels of scumming than the other surfaces. This trend is repeated with the other ink and substrates. Again however, the other surfaces show similar levels of scumming.

An interaction was also observed between surface finish and ink type, Graph 5.6. Here clearly different results are obtained using different ink types – a low scum ink, and a normal NC ink.

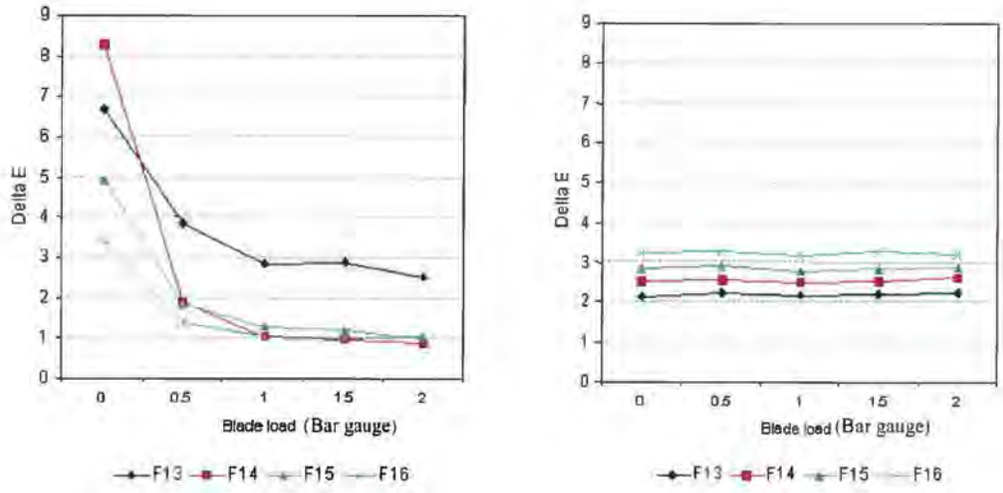

Ink 3 Ink 4 (low scum ink)

Graph 5.6 – Effects of blade load. Cylinder 3, red inks, white OPP

Graph 5.6 shows the effects of changing the ink on cylinder 3. Considering ink 4 (the low scum ink), the finishes are clearly ranked in terms of scumming level, as F13, F14, F15 and F16, from best (least scumming) to worst (most scumming), and in this case, doctor blade load has had no clear impact on scumming levels, and this is in sharp contrast to the other results. The reasons for this are unclear and require further investigation. A possible reason is that ink transfer at the cylinder-substrate junction is inhibited in these ink systems. This will be considered further in Sections 5.5 and 5.6. Considering ink 4, not only is significantly higher scumming observed than with ink 3, but the surface finish ranking has been reversed, with F16 providing the best (lowest) level of scumming and F13 providing the worst (highest) level of scumming. This is, as stated, due to an interaction between ink type and surface finish. Due to the nature of these variables, this cannot be quantified, without further exploration, for example, into the effect of different ink components, and this requires further work.

The findings shown in Graph 5.4, Graph 5.5 and ink 3 in Graph 5.6 are due to the techniques involved in cylinder surface polishing. Stone polishing is performed using a stone disk, which rotates at high speed in close proximity to the cylinder. Paper is vibrated against the side of the cylinder, but is drawn from a belt. As the stone is used, any particular protrusions are rapidly worn off, leaving a relatively regular surface. This produces an approximately even surface, with approximately equal numbers of

peaks and troughs. The area of the paper being used constantly changes, with new paper being brought into the engraving area. As a result, there is a significant difference in the form of the surface between those polished with a stone or paper polisher. Paper polished surfaces show a significantly larger number of large troughs than observed with a stone polished surface.

To support this, both papers and stones were analysed using interferometry to examine their surfaces as shown in Figure 5-6, below. The stone surface was relatively smooth, with a roughness (Ra) value of approximately 5um. In comparison, the roughness of the paper was in excess of 20µm. The consequent effect on the copper finish can be seen in Graph 5.7. . It can be seen that the paper finished surface exhibits significant troughs, while the stone finished surface exhibits more peaks, which will rapidly wear off on printing.[22] It is this extra roughness, caused by the continuous replenishment of the paper that has led to the greater concentration of troughs in the paper polished surface, which has, in turn led to the increased scumming levels observed using this finishing technique.

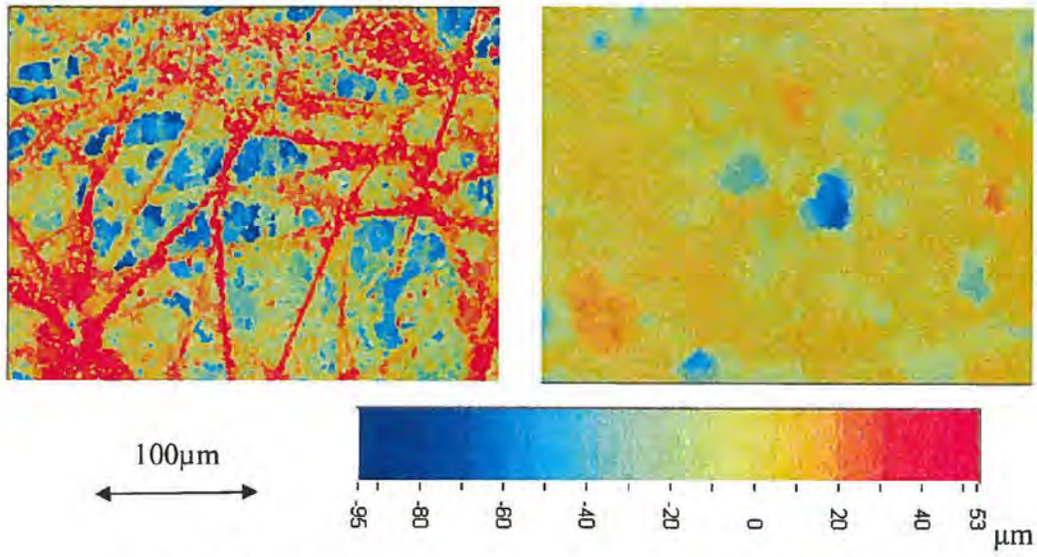

Figure 5-6a - Paper

Figure 5-6b - Stone

Figure 5-6 – Polishing surfaces, used materials

[22] No scale is shown for Figure 5-7 as the scales are different. However, green has been set to show the mid level in each case. Thus the predominance of red in the stone finished surface indicates peaks, while the predominance of blue in the paper finished surface indicates troughs.

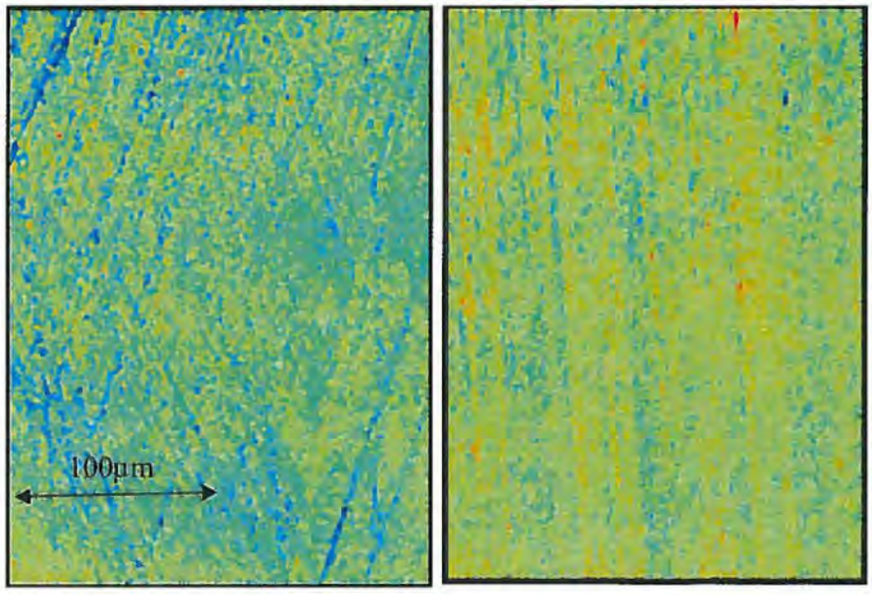

Paper finished copper Stone finished copper

Figure 5-7 – Copper surface after polishing

Although the absolute roughness of the polished surface (within practical limits) has little bearing on the levels of scumming observed in the final printed substrate (see Graph 5.4), the form of the finish does. Also, the type of polishing used on the copper affects the level of scumming far more than the polishing of the chrome. This is largely due to the softness, and smoothness of the copper supplied for polishing. The raw copper, taken from the polishmaster is extremely smooth, but is also extremely soft (HV50-70). This surface is highly 'roughed up' by the polishing action. Once the copper has been engraved and chromed, the top surface is much harder (HV900-1100), and the polishing materials alter the surface much less than they do to the copper surface. Thus the effect of polishing material on the chromed surface is much less than the effects on the copper, and this is reflected in the trends shown in Graph 5.1 and Graph 5.2.

An interaction was observed between blade load and average scumming levels and surface finish, Graph 5.7, where at lower blade loads, the smoother surfaces (cylinder 2) exhibit a higher level of scumming, whilst at higher blade loads they exhibit a lower level of scumming. This is attributed largely to the surface roughness. Smoother

surfaces ensure that a larger area is available for hydrodynamic action, so the film thickness is increased, and more ink passes there. Rougher surfaces ensure that there are contact points (asperities) between the blade and the cylinder and ink passes through in the valleys between. In this circumstance, the ink flow under the blade due to hydrodynamic action exceeds the ink flow in the roughness grooves. At higher blade loads, the coefficient of friction between the blade and the cylinder is significantly higher (see Figure 5-1). This is likely to lead to increased blade deflection, which allows a greater flow under the blade when approaching the maximum flow region (identified as 'C' in Figure 5-2).

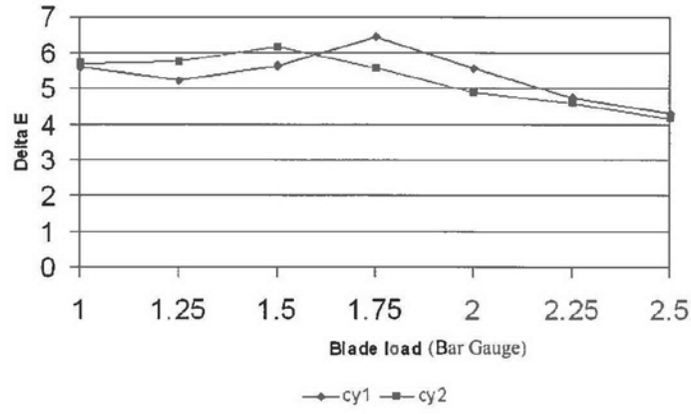

Graph 5.7 – Average scumming with each cylinder. White OPP, PVB ink

The graphs (Graph 5.4, Graph 5.5, Graph 5.7) also include the effect of load, where a peak in ΔE occurs at about 1.5 or 1.75 bar loading cylinder pressure. This suggests a thicker film is being deposited and reflects the peaked region 'C' as depicted in Figure 5-2, lending support for the application of this model to characterise scumming behaviour.

In addition, it can be seen that the 'C' peak (Figure 5-2) is significantly more pronounced on the two paper finished surfaces (F1, F6). It is likely that this is caused by the additional ink carried on these two surfaces compared with the others. As the coefficient of friction is significantly higher on these surfaces (due to the increased surface roughness), it is far more likely that the surfaces are operating in the boundary lubrication range, which will cause the blade to bend far more significantly. In

addition, these surfaces have shown the greatest degree of wear during printing. This is consistent with lubrication theory.

In summary, the effects of surface finish are small, providing that an operability window has been maintained, but that extremely rough surface finishes will lead to elevated scumming levels. The effects of surface finish are small when compared with the effects of blade load and ink. These issues will be discussed in further detail below.

5.4 Effect of blade load

The preceding section has illustrated the importance of blade load on scumming. This section examines in more detail the blade load in terms of the gauge pressure applied to the loading cylinder, but also references the actual applied load. The blade had a number of strain gauges bonded to it, in order to accurately ascertain the actual load being applied to the cylinder by the blade.

Several different regimes were observed when analysing the effects of varying blade load on the measured scumming levels, and have been shown in Graph 5.8. In some cases, a 'threshold response' was observed, where little scumming occurred until the blade load dropped below a 'threshold level', suddenly allowing ink to pass under the blade. In other cases (particularly the 'low scum' ink) blade load was not found to have a significant effect, with scumming remaining constant at all blade load levels, but in most cases a curve was observed, with a defined peak, and this is referred to as a 'bell shape' in the following paragraphs.

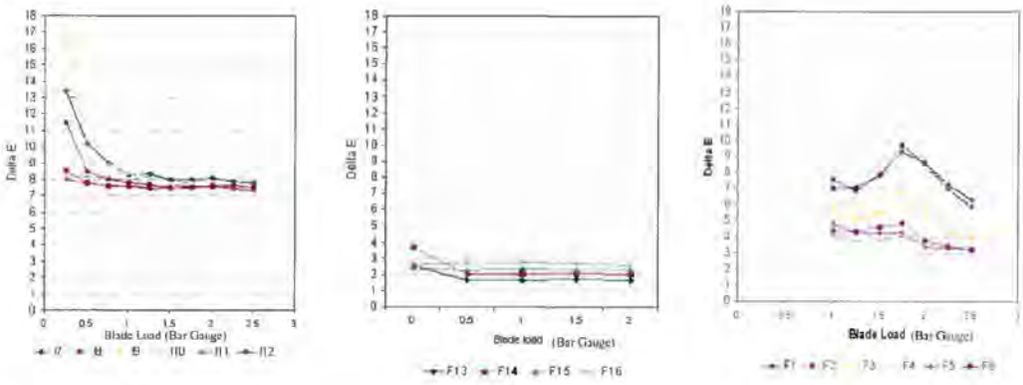

Threshold Response (A) No Response (B) Bell Curve Response (C)

Graph 5.8 – Response curves to blade load changes

The bell shaped curve occurred on many of the substrate / surface / ink combinations. It was characterised by a general increase in scumming as the blade load was decreased from a maximum, with a slight decrease observed at some point in the blade load reduction, and then a significant increase in the observed levels. These reflect the trends shown in Figure 5.2 and this suggests that the model proposed in [23] is appropriate to characterise aspects of scumming that are determined by doctoring performance.

As explained in Section 3.3.2.3, strain gauges were bonded at points across the blade. Values for strain taken from these gauges are shown in Graph 5.9. Nine different blade load settings are shown, spaced approximately as indicated by '1' to '9'. Large blade deflections are shown as large negative values of strain (ie 1 – 3). It can be seen that little change in blade surface strain occurs between points 1 – 3 in the graph despite approximately linear increases in air supply pressure to the loading cylinder. As the supply pressure is then decreased, the blade becomes less deflected, and this is measured as the difference between the blade load at points 3 and 4.

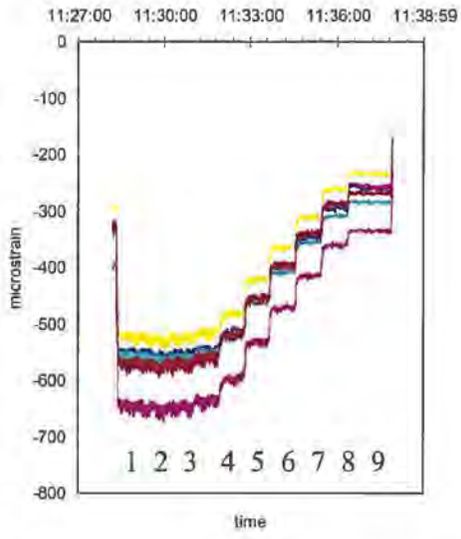

Graph 5.9 – Blade deflection – typical values

Blade load was found to have no significant effect on the levels of scumming using the 'low scum' ink. Discussion with the manufacturer of the ink indicated a lack of adhesion promoter being added to the ink, this lack of adhesion promoter being attributed to the lack of scumming observed. It is known that there is a minimum cell size for a specific ink to be able to transfer ink to the substrate surface. This work has indicated that the cylinder surface is acting, in effect, as a series of micro-cells, carrying ink under the blade to the substrate surface, and that these surfaces 'print' the ink across the entire substrate, but at levels low enough not to be visible. When scumming occurs, these cells are carrying more ink, enough this time to be properly transferred to the substrate surface. In the case of the 'low scum' ink, these cells never get big enough to transfer enough ink to be a visible level of scumming, partly due to the release characteristics of the ink / cylinder combination, and partly to do with the reduced adhesion characteristics of the ink.

Threshold results were primarily noted on the metallised film, but were also observed during the second trial (using cylinder 3, see Graph 5.6). Here, the surface of the film is significantly different to the surface of either the clear or white films, due to the presence of a 'white base' having been previously printed onto it. Subsequent analysis of these 'threshold response' curves indicates a flattened blade load response, (with the peak at 'c' in Figure 5-2 being significantly lower than suggested by Figure 5-2)

very similar to the responses described previously, with the variation that the increase caused by the blade bending has made very little difference to the scumming level.

If blade load is converted to actual applied load, using the strain gauge data [61] [62] very similar results are seen, with the threshold becoming significantly more obvious, Graph 5.10. It is also noticeable that the threshold occurs at a finite load (approximately 600N). This is applied directly by the weight of the holder and corresponds to a cylinder pressure of 0bar gauge.

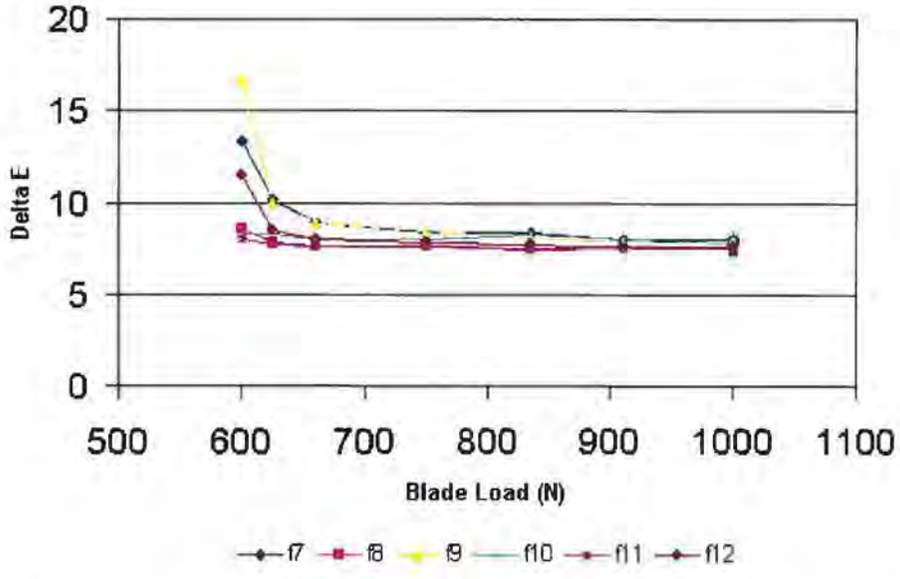

Graph 5.10 – Blade load and Delta E. Blade load converted to N. Same data as Graph 5.8A

In summary, under most conditions, the effects of blade load are extremely significant, exhibiting a much greater effect than the differences seen between surface finishes.

5.5 Effect of Substrate

Changing the substrate has a significant effect on the levels of scumming observed, both in terms of the overall level, and in the form of the scumming. Using basic image analysis, it was confirmed that two clearly different forms of scumming occur,

between the white OPP film, and the metallised film, with a white base on it, Figure 5-8.

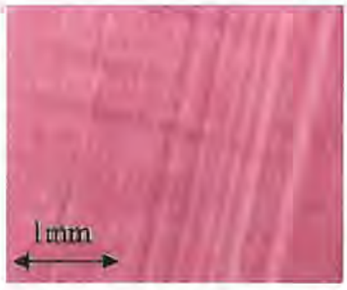

Figure 5-8a – OPP

Figure 5-8b - Metallised

Figure 5-8 – Forms of scumming (60x magnification)

It can be clearly seen that two different forms are occurring. On the OPP film, there is an even covering of ink, with apparent clear lines through it, which were identified as extrusion defects[23] while the metallised foil shows a more random pattern of dots, with clear patches, and much denser patches. It was not possible to analyse this effect using the white light interferometry technique used in the analysis of printed dots, as these dots were too small to be identified among the surface roughness of the substrate.

The random patterns observed in the metallised foil are caused by the surface energy of the substrate. The white base applied to the metallised foil has a significantly lower surface energy than the OPP substrate[24]. This has led to the ink reticulating as the micro-dots coalesce.

---

[23] Examination with white light interferometry identified the cause of the lines visible in the OPP substrate. During manufacture, as the film is extruded a series of ridges, with a wavelength of approximately 25μm are also extruded (indicated with the arrow). Furthermore, a larger wave is observed with a wavelength of varying between approximately 100-180μm.

[24] This was measured using a set of dyne pens, which provides a comparative result between the substrates being examined.

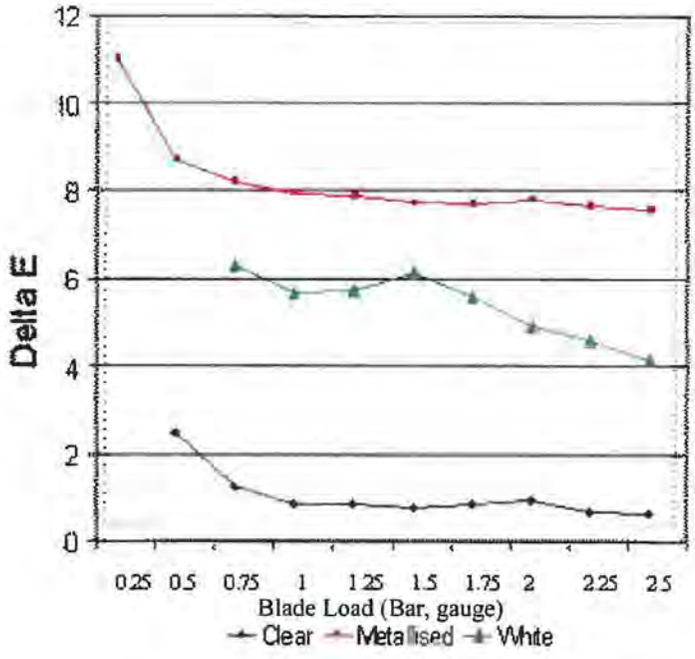

Graph 5.11 – Effects of substrate, averaged effects for cylinder (cylinders 1 and 2) and black ink (PVB and NC)

Graph 5.11 (above) shows the effects of changing substrate on scumming levels. It is clear that not only does changing the substrate change the level of scumming, but that it also changes the response observed. The clear substrate demonstrates the lowest level of scumming, while the metallised foil demonstrates the highest levels of scumming. Both however, demonstrate the 'threshold' response, where blade load has little effect on the scumming above a certain 'threshold' level. On closer investigation however, it can be seen that there is still a blade coating response, although this is most marked on the white substrate. The reasons for this behaviour are not clear for these experiments. Possible causes may be attributed to substrate surface energy levels, and this requires further investigation.

5.6 Effect of ink type

Several different inks were examined over the two trials. The first trial considered an example of each of the primary ink systems, nitrocellulose (NC) based system and a polyvinyl butyral based (PVB) system (inks 1 and 2 respectively, Graph 5.12). The

second trial used three NC inks (as the most common system used), inks 3, 4 and 5. Although the base for inks 1, 3, 4 and 5 is common, they are significantly different inks, with different solvent bases, different pigments and additives.[25]

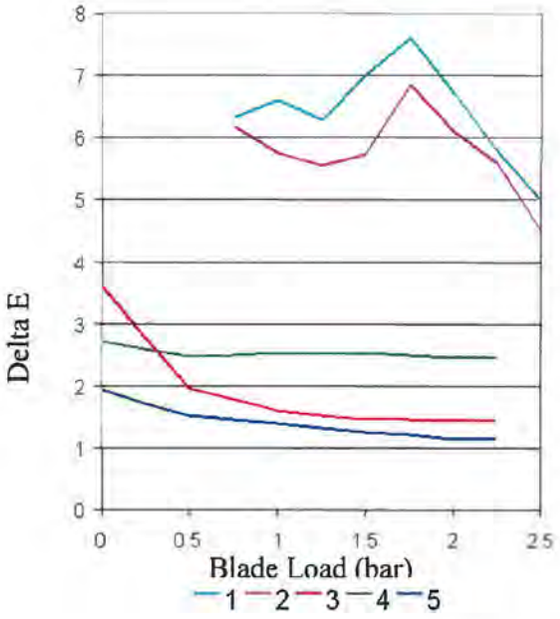

Graph 5.12 – Effects of ink system

Two clearly different regimes are observed when average scumming levels for all conditions are plotted against ink type. Inks 1 and 2 were used in the first trial. It can be clearly seen that higher levels of scumming are observed (partly a function of the substrates being used) and that a significant bell curve is observed.

The other inks (used in the second trial) all exhibit lower levels of scumming. Generally ink 4 (the low scum ink) exhibits the highest level of scumming across the load range. This was however, independent of blade load. This insensitivity to conditions should make a minimal level of scumming obtainable more easily than with the other inks in difficult conditions. The characteristic of the 'bell shape' is not easily visible with these inks. As discussed earlier this may be due to the characteristic residing in the leftmost region of the curve in Figure 5-2, or the fact that

[25] It should be noted that the surface finishes between the two trials are comparable. See Figure 5.3 and Footnote 12 for details.

ink still passes under the doctor blade and the 'low scum' alteration to the ink makeup inhibits transfer at the printing nip

Finally, it is clear that the ink is a significant variable in the scumming process, affecting not only the level of scumming, but also the type of response observed, and the manner in which the surface finish affects scumming (Section 5.3.2).

5.7 Effect of viscosity

The effects of viscosity were investigated by running a set of trials utilising inks of various viscosities, ranging from 25s (Zahn 2) to 17s (Zahn 2), using conventional reduction techniques. The effects of viscosity on each of the surface finishes is shown in Graph 5.13.[26]

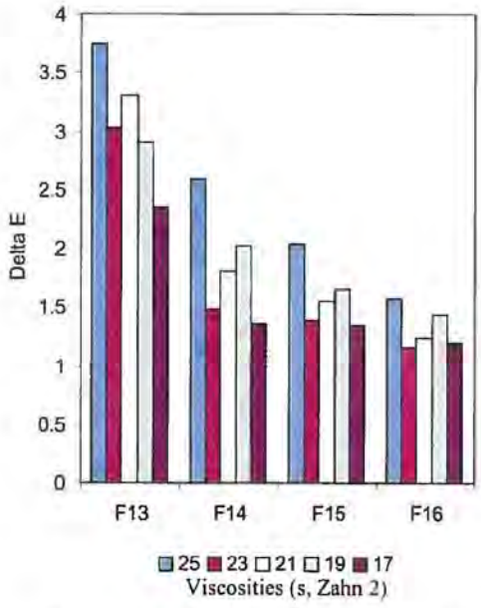

Graph 5.13 – Viscosity effects with surface finish, clear OPP, red ink. Viscosities given in seconds, Zahn 2

[26] The surfaces of the cylinder exhibit significant wear over the course of the trials (see Graph 5.1 and Graph 5.2). The results given in Graph 5.13 are averaged over the course of the entire trial, utilising results from both the start (unworn cylinder) and the end (worn cylinder) of the trial, thus removing the influence of wear on the cylinder.

Overall it is seen that as viscosity decreases, the level of scumming decreases, although within the experiment there is an increase in scumming between the 23s, 21s and 19s viscosity inks, before decreasing again between 19s and 17s. The scumming level change between 25s and 17s is significant, with maximum differences of $\Delta E=1.5$. This is a significant, visible colour change, whilst the changes observed at intermediate levels are not large enough to be visible under normal viewing conditions.

Significant differences were also observed with the surface finish. While F16 does not show a significant variation in scumming levels as viscosity is changed, F13 shows a reduction in scumming of $\Delta E=1.5$ between the highest and lowest viscosities. An interaction was also observed between the surface finish and the ink viscosity. Some of the surfaces (F15, F16) did not show significant variation between the extremes of viscosity, while others (particularly F13) did. Since F13 is significantly the roughest surface, it is likely that this is related to the grossly elevated surface roughness, with this allowing more ink to pass under the blade.

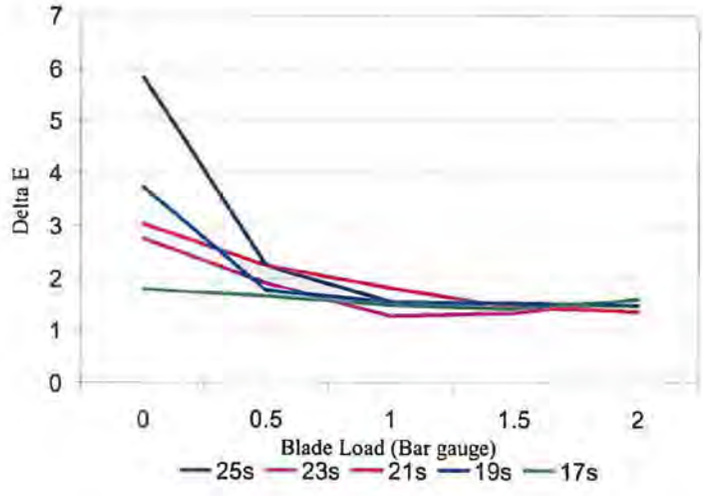

Graph 5.14 – Viscosity effects with blade load

There is a general trend, where in each case, the high viscosity ink produced significantly more scumming than that produced with the lowest viscosity inks. The

response is also non-linear. Higher viscosity inks provide significantly increased hydrodynamic forces, forcing the blade away from the cylinder, whilst lower viscosity inks produce much lower forces. If the force applied by the blade remains constant, and since (according to Newton's third law) all forces must be balanced, if the viscosity decreases, there will be a lower hydrodynamic force, thus requiring the film thickness to drop until equilibrium is reached again. Increasing the viscosity has the opposite effect. This lower film thickness with lower viscosity inks leads to lower levels of scumming.[27] This is an interaction between blade load and ink viscosity.

It was also observed that varying the viscosity of the ink alters the position of the 'peak' in the 'bell curve response', Graph 5.15.

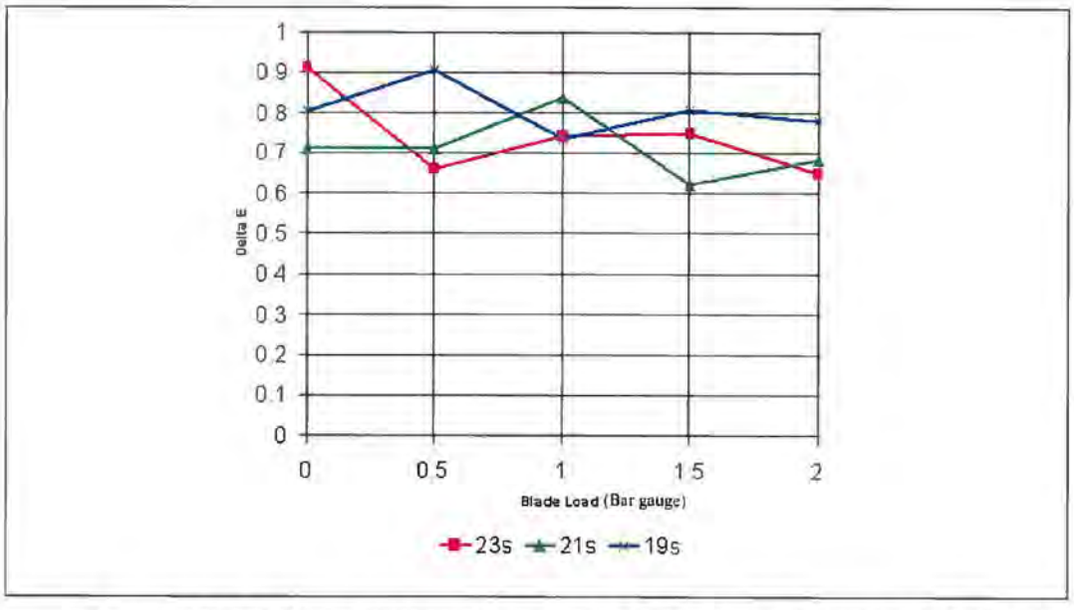

Graph 5.15 – Effects of viscosity on peak of bell curve. Averaged ink effects, white OPP.

This shows a section of the curve. The peak in the characteristic for the 23s (zahn 2) ink is observed at 1.5Bar (gauge) blade load.[28], while the peak for the 21s ink is at

[27] Lower viscosity inks also have a lower colour strength, due to the increased quantity of solvent added, however, this is a small difference compared to the film thickness variation.

[28] The extra peak in the 23s curve is the point 'a' in Figure 5-2 – where the blade is straightening.

1Bar, and the 19 second ink at 0.5Bar. This indicates that as viscosity increases, the peak of the curve moves towards higher blade loads. The hydrodynamic mechanisms that cause this have been discussed above.

5.8 Closure

Although it is widely believed that the surface finish of a gravure cylinder is the largest variable affecting scumming, it is only one of several parameters.

The widely used practice of 'roughing up' cylinders with emery paper, far from 'roughing up' the surface actually smoothes it.

The type of polishing used on the copper surface has a large effect on the scumming levels, and that this has a far more significant effect than the absolute roughness values, with the 'direction' of the roughness (either above or below the mean line) being significant.

A response similar to that observed in blade coating is observed in scumming levels. This is caused by deflection of the blade by the normal forces caused by the fluid (ink) attempting to flow under the blade. The effects of varying the ink viscosity have also been discussed, and the effects detailed with reference to the effects of blade load, indicating that much larger effects are observed when using lower blade loads.

The effects of varying the substrate altered not only the levels of scumming, but the form of scumming observed, with white base coated metallised foil showing larger patches of ink transferred than the extremely thin, even coating observed on both the white and clear films. Changing the ink type affects the level of scumming, with the NC ink offering lower levels of scumming across most of the blade load range, but that the PVB ink shows a continuing decrease as blade load is increased, and were that trend to be continued, lower levels than observed could be expected.

Chapter 6

Conclusions and Recommendations

This research has dramatically increased the understanding of ink release in the rotogravure printing process. A search of the available literature has shown a distinct lack of fundamental understanding of the process, with little relevant literature relating to the precise quantities of ink transferred from the image carrier, and no scientific investigation into the causes of 'scumming' despite its relevance as an industry wide problem.

This research is the first to properly analyse the three dimensional cell geometry, and has necessitated the development of a technique to perform this measurement. Further techniques have also been developed to analyse the volume of the printed dots and the quantity of retained solvent in the dots. Only by understanding how big the cells actually are, and how large the printed dots are, can one begin to understand how much ink is transferred, and to understand how the various factors affecting electromechanically engraved cells will affect this transfer.

The research is also the first to properly investigate the many factors affecting scumming in the gravure process, and the effects of several variables have been qualified.

By carrying out these trials on production presses, using standard, production substrates and using conventional production inks, the implications of this research are of value to anyone working in the modern rotogravure industry. The conclusions of this research are detailed in the first section of this chapter, whilst recommendations for continuations of the work are proposed in the second section.

6.1 Conclusions

6.1.1 Ink release from image areas

- A technique has been developed to accurately quantify both cells and printed dots, in terms of their volume and geometric parameters, with an accuracy of ±0.3% of cell volume to ±0.1% depending on cell size (the larger the cell, the more accurate the measurement, using a specified tolerance of ±40μm^3 / measurement)
- The volume of a cell has been shown to differ significantly (a maximum of approximately 60%) from traditional methods of volume calculation using image processing. This demonstrates a problem in engraving understanding, which is remedied by
- An improved technique for volume calculation using image processing has been demonstrated, which is accurate at approximately 80% coverage. This allows engravers to make a much better calculation of cell volume for accuracy of engraving.
- The direct relationship between cell depth and width has been demonstrated.
- It has been shown that as screen ruling is increased, the shape of the cells is maintained, with the size of the cells merely being scaled down.
- It has been shown that as compression ratio is increased, the length of the cells increases and the width decreases. The volume remains approximately constant up to 45°, but decreases if compression ratio is increased further.
- It has been shown that as stylus angle increases, the width, length and open area of the cell remains constant, and that the depth (and thus the volume) decrease.
- This work has provided a tool to the engravers who can calculate their gamma curves reliably, and with a hitherto unavailable degree of accuracy. This aids the industry as it allows for cylinders to be 'right' first time, every time.
- It has been shown that dry ink contains approximately 1% retained solvents by volume, and can thus be ignored in future studies.
- This work has calculated ink release from gravure cells, and has shown it to be 18.3% of the total cell volume, ±2.5%, depending on the specific conditions.

- It has been shown that release increases slightly as compression ratio, stylus angle and screen ruling increase. This allows for designs to be optimised for maximum (or minimum) ink release for a specific image, which allows for better colours in the packaging (or publishing) market.
- The differences between this work and previously calculated values have been shown to be due to (a) inaccuracies in previous measurements, and (b) unrealistic inks and printing conditions being used in previous experimental research, as when a correction factor is applied (to compensate for volume miscalculation) results are very close to those calculated.

6.1.2 Ink release from non-image areas

- A technique has been developed to accurately quantify scumming on both transparent and opaque surfaces that is both analytical and methodical, in comparison with previous private studies which have only examined one parameter. The understanding of the effects of several variables have been quantified, and their interrelationship identified.
- The lack of understanding regarding cylinder preparation has been demonstrated and it has been shown that the cylinder, during manufacture gets smoother, and that applying emery cloth to the finished cylinder to 'rough it up' actually make it smoother, giving a better wiping surface, and eliminating scumming by improving the wipe, rather than allowing a better lubricating film under the blade.
- A level of scumming is always observed between the printed and unprinted substrate. Only when this level reaches visible levels is it problematic.
- It has been shown that the level of scumming is affected by blade load. Generally a lower blade load will allow more ink to pass under the blade, leading to higher levels of scumming, but not always, as discussed in sections 5.2 and 5.4. Increasing blade load will, however always lead to an increase in cylinder and blade wear, possibly requiring jobs to be 'pulled' and cylinders remade.
- It has been shown that there is a significant correlation to the well understood process of blade coating.

- It has been shown that the level of scumming is affected by the surface finish of the cylinder. Although there is no direct correlation between the roughness statistics of the cylinder surface finish and the scumming level, both the form and the structure of the surface have a large effect on the level of scumming observed, with paper finished cylinders causing more scumming than stone finished.
- It has been shown that the surface roughness of the cylinders does not affect scumming levels significantly unless gross changes occur in surface roughness, thus engravers do not need to be so precise in the production of an extremely accurate R_a value on the surface finish, and that considering the profile which is polished into the finish is more appropriate to managing scumming levels
- It has been shown that the level of scumming is affected by the ink and the substrate being used. This result is not quantifiable because there is no analogue between the different types of substrate / inks. The effects of changing the substrate are large, affecting both the response and level of the scumming. The effects of changing the ink are particularly critical however, and are by far the dominant variable in the level of scumming.
- It has thus been shown that there is an interrelationship between variables, and that while it is possible to operate at a variety of different conditions, changing one variable, may unpredictably alter the scumming level in the process, removing the 'balance' of the variables in the process.
- This work provides a tool to allow printers and engravers to work together to minimise the possibility of scumming occurring, and will enable them to remove it rapidly, and identify the causes should it occur, to prevent this happening repeatedly.

6.2 Recommendations for further work

- The work needs to be extended to measure the release over more of the coverage scale. It has only been possible to measure between 30% and 50% coverage due to the requirement for the individual dots to not be joined. As a

result, it is necessary for the work to be extended to both lower and higher coverages.

- The work should also be extended to investigate release onto porous substrates. Non-porous substrates were chosen to ensure that no penetration of ink occurs. This allows the volume of ink transferred to be ascertained from the volume of dry ink on the surface. It is suspected that the release characteristics when printing onto porous substrates will be significantly different than onto non-porous substrates.
- While the value of ink release has been calculated, assuming 95% full cells, based on the work of Kunz [25] the filling state of the cells should be ascertained experimentally, and under production conditions.
- The investigation into the effects of scumming should be continued. Both in terms of investigating the effects of porous substrates, and in an attempt to quantify the effects of the variables on the levels. This research has identified a series of variables which should be examined in further detail, particularly the effects caused by the ink. A trial should be run to examine the effects of changing ink components, particularly the adhesion promoter.
- The effect of surface finish condition should also be investigated to investigate how wear occurs to the cylinders during the long print runs common to the industry.
- The effects of scumming when printing multiple colours should also be investigated. It is unusual for a gravure print job to be of only one colour, and as such it is needed for investigation to examine the effects of scumming when printing a multiple colour job.

References

1. UK Environmental Technology Best Practice Programme, 1998 (ETBPP)
2. Key Note Report, Key Note Market Information Centre, 2001
3. C. L. Kasunich "Gravure Primer" GATF 1998
4. http://www.spectron.co.uk/Pages/datwyler.html
5. M. Hirata, D. Tang, K. Nonami, H. Ogawa and Y. Taniguchi "Ultra-high speed positioning control of a gravure engraving unit using a discrete-time two-degree-of-freedom H_T control" Control Engineering Practice No. 10, 2002, pp783-795
6. D. Joehnk "The impact of Electron Beam technology (Heliobeam)" ERA Conference proceedings, 1992 pp 67-76
7. Gravure Association of America "Gravure Process and Technology" GAA 1991
8. G. Hennig, J. Frauchiger "New engraving technique opens up new perspectives for rotogravure printing" Flexo and Gravure Asia, 1-2002 pp6-9
9. Private communication with Tronic Gravure Ltd
10. Private communication with Teich Flexibles Ltd
11. Information supplied by BASF Printing Systems Ltd
12. B. Massing and M. Schaeffeler "Flexo and gravure inks for packaging printing – comparison of ink systems" Flexo and Gravure International, No. 1, pp20-22, 2002
13. Private communication with Daetwyler UK Ltd
14. "Increasing quality and reducing waste with coated doctor blades", Flexo and Gravure Asia, Vol. 1, No. 1, pp62-63, 2002
15. R. W. G. Hunt "Measuring Colour" 2nd edition, Ellis Horwood 1991
16. G. G. Field "Colour and its Reproduction" 2nd edition, GATF Press 1999
17. Hunt R. W. G. "Measuring Colour" 3rd Edition, Fountain Press, Kingston on Thames, 1998
18. From www.x-rite.com
19. A. Murray "Monochrome Reproduction in Photoengraving" Journal of the Franklin Institute, Vol. 221, No. 6, pp 721-744, 1936
20. J. A. C. Yule, W. J. Nielson, "The Penetration of Light into Paper and its Effect on Halftone Reproductions" TAGA Proc. 1951, pp 65-76
21. Fox, I. J. "Characterisation of Prints Using Image Analysis Methods" MPhil Thesis, UW Swansea, 1999

22. Bohan M. F. J., Clist, A. M., Claypole, T. C. and Gethin, D. T. "Characterisation of Gravure Cylinders' TAGA 2001
23. B. Griffiths "Manufacturing Surface Technology" Kogan Page Science, 2000
24. S. Lippold and J. Podlesny "WYKO Surface Profiles Technical Reference Manual", Veeco Metrology Group, 1998
25. W. Kunz "Ink transfer in gravure process" TAGA 1975
26. W. R. Bowen, T. Doneva, N. Hilal and C. J. Wright, "Atomic Force Microscopy: Images and Interactions" Microscopy and Analysis, January 2001, pp5-7
27. W. R. Bowen, N. Hilal, R. W. Lovitt, C. J. Wright. "Atomic Force Microscopy" Encyclopaedia of food technology, (eds. R Robinson, C Batt and P Patel), Academic Press, 1999, 1418-1425
28. http://www.cmmp.ucl.ac.uk/~atg/work/stm.htm
29. S. F. Kistler and P. M. Schweizer "Liquid Film Coating", Chapman and Hall, 1997
30. Private communication with Veeco UK Ltd.
31. De Hoffman, E., Charette, J., Stroobant, V. "Mass Spectrometry, Principles and Applications" J. Wiley and Sons, Chichester, 1994
32. Montaudo, G., Lattimer, R. P., "Mass Spectrometry of Polymers" CRC Press, Florida 2002
33. Private communication with Markes International
34. "TurboMatrix thermal desorption systems", Advertising brochure, Perkin-Elmer instruments, Connecticut USA, 2002
35. http://www.markes.com/TechnicalHelp/ThermalDesorptionOverview.asp
36. "Clarus 500 Gas Chromatograph/Mass Spectrometer", Advertising brochure, Perkin-Elmer Instruments, Connecticut USA, 2002
37. Garcia M.A. and Sanz J. "Analysis of Origanum vulgare volatiles by direct thermal desorption coupled to gas chromatography-mass spectrometry" Journal of Chromatography A, 918 (2001) pp189-194
38. Bohan, M.F.J., Claypole, T.C., Anderson, J.T., Jewell, E.H. and Gethin D.T. "The use of Orthogonal Array Techniques in Printing Research" Pan-Pacific and International Printing and Graphic Arts Conference, Quebec, 1998
39. M. F. J. Bohan, T. C. Claypole and D. T. Gethin "The effects of process parameters on product quality of rotogravure printing" Proc Instn Mech Engrs Vol 214 Part B, 2000

40. M. F. J. Bohan, T. C. Claypole and D. T. Gethin "An investigation into Ink Transfer in Rotogravure Printing" TAGA Proc. 1998
41. S. Elsayed, F. Morsy, S. El-Sherbiny, E. Abdou "Some factors affecting ink transfer in gravure printing" Pigment and resin technology" Vol. 31, pp234-240, 2002
42. H. Benkreira and R. Patel "Gravure Roll Coating of Low Viscosity Liquids" JOCCA, Vol. 75, No. 7, pp261 – 268, 1992
43. H. Benkreira, R. Patel, M. Naheem, J. M. LeClercq "Film thickness and instabilities with forward gravure coating" from "The Mechanics of Thin Film Coatings", editors P. H. Gaskell, M. D. Savage and J. C. Summers, pp213 – 220, World Scientific, Singapore, 1996.
44. W. W. Pulkrabek and J. D. Munter "Knurl roll design for stable rotogravure coating" Chemical engineering science, Vol. 38, pp1309-1314, 1983
45. A. Pekarovicova, J. Pekarovic, M. Joyce and V. Khunova "Phase Change Inks for Rotogravure", Taga proceedings, 2002
46. J. F. LaFaye, J. P. Maume, J. M. Schwob, R. Chiodi "The effect of some coating variables on gravure print quality using lightweight coated paper" Tappi Journal, Vol. 71, pp63-69, 1988
47. H. U. Heintze "Press operation and gravure print quality" Tappi Journal, Vol. 65, pp109-112, 1982
48. P. Hansson and P. Johansson "Topography and Reflectance Analysis of Paper Surfaces using a Photometric Stereo Method" Swedish Pulp and Paper Research Institute
49. P. Hansson and P. Johansson "A new method for the simultaneous measurement of surface topography and ink distribution on prints" Swedish Pulp and Paper Research Institute
50. S. Tucker "Interferometric anilox volume measurement" Flexotech, May/June 1997, pp22-23
51. C. Hine "Anilox Rolls are Key When Printing Corrugated Board" Paper, Film and Foil Converter, August 2000
52. H. Benkreira and O. Cohu "Direct forward gravure coating on unsupported web" Chemical Engineering Science, Vol. 53, No. 6, pp1223-1231, 1998

53. D. R. Jeske "Impulse Press Simulation Of A Gravure Printing Nip" 1990 International Printing and Graphic Arts Conference, Vancouver, British Columbia, Canada, Nov. 6-8, 1990, pp97-104
54. N. Kapur, P.H. Gaskell and A. Bates "A Parametric Study of Offset Gravure Coating" Trans IChemE, Vol. 79, Part A, pp41-50, Jan 2001
55. H. Benkreira and R. Patel "Direct Gravure Roll Coating" Chemical Engineering Science Vol. 48, pp2329-2335, 1993
56. L. W. Schwartz "Numerical modelling of liquid withdrawal from gravure cavities in coating operations; the effect of cell pattern" Journal of Engineering Mathematics, Vol. 42, pp243-253, 2002
57. C. A. Powell, M. D. Savage and J. T. Guthrie, "Computational Simulation of the Printing of Newtonian Liquid From A Trapezoidal Cavity" International Journal of Numerical Methods for Heat and Fluid Flow, Vol 12. No. 4, 2002
58. Bohan, M. F. J., Claypole T. C., Gethin D. T., "An Investigation Into The Effect of Process Parameters On The Ink Supply Characteristics To A Roller Train In An Offset Printing Press" Journal of Prepress and Printing Technology, Vol 3, March 1999
59. Phadke, M. S. "Quality Engineering Using Robust Design", Prentice Hall Int, 1989
60. Grove, D.M. and Davies T.P. "Engineering Quality and Experimental Design", Longman Sci. and Tech. 1992
61. Private communication with T. V. Korochkina, WCPC, 2002
62. Private communication with M. F. J. Bohan, WCPC 2002
63. Private communication with Tecnograv Group Ltd
64. Private communication with Brand Packaging Ltd
65. Private communication with Amcor – Colodense Ltd
66. Private communication with Printpack UK Ltd
67. Hubschmann, H-J. "Handbook of GC/MS" Wiley, New York, 2000
68. Chatfield, C. "Statistics for Technology" Chapman and Hall, 3rd ed, London, 1983

A1 Appendix 1 – Diamond Measurements

A1.1 Diamond analysis

A typical engraving diamond in its mount is shown along with an engraving head in Figure A1.1. It is shown that the diamonds used in engraving have a significant effect on the geometry of the cells engraved. Historically, diamonds have been examined in terms only of their angle, measured using a projected shadow. Further analysis was required in order to ascertain the precise geometry of the engraving diamond used in the engraving process.

Interferometric analysis was used in order to define the shape and hence the condition of the diamond, in terms of its angle, the condition of its face (cutting) surface, the wear of edges and the wear of the tip. Previously no method has existed to analyse these features, and so a new methodology was developed. This is discussed in the following sections.

Figure A1.0-1 – Engraving Head and Diamond

Measurements were taken using different levels of magnification – 10x, 20x and 40x. These results were all taken using the same calibrated lens to remove the possibility of bad data due to inaccuracies between lenses.

A1.1.1 Stylus Angle Calculation

As shown in Figure A1.0-2, Stylus angles were calculated manually from interferometric measurements. Specifically, in an initial analysis, the alignment of the two sides of the cutting face (a and b in Figure A1.0-2), were measured manually, and the resultant angle was taken from the analysis package. On repeated measurement of diamonds following a period of engraving, it was discovered that the stylus angle decreased with used, despite the ultimate hardness of this natural material. A second test was then instituted to examine the angle with reference to a fixed surface, 'c' in Figure A1.0-3. Because this surface never enters the copper surface of the cylinder it should never experience wear, and therefore provides a good reference surface for comparison of the other sides.

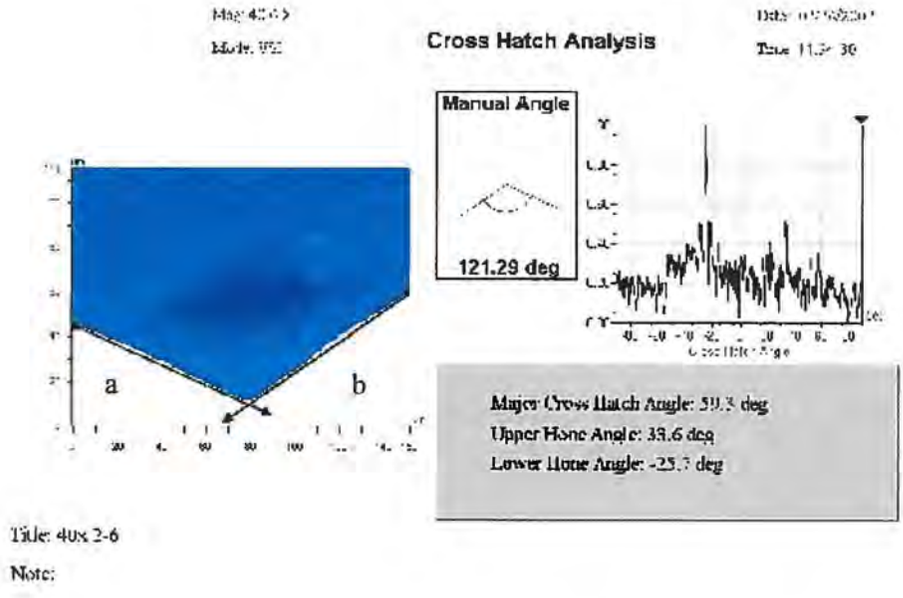

Figure A1.0-2 - Cross Hatch Analysis

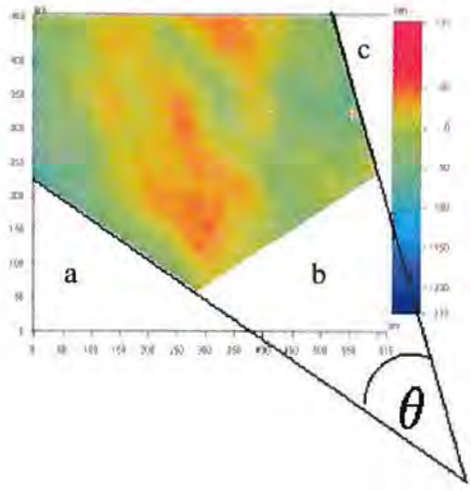

Figure A1.0-3 – Angle evolution analysis

The angle θ was calculated and provides a reference over the life of the diamond. The evolution of stylus angle itself is shown in Graph A1.1.

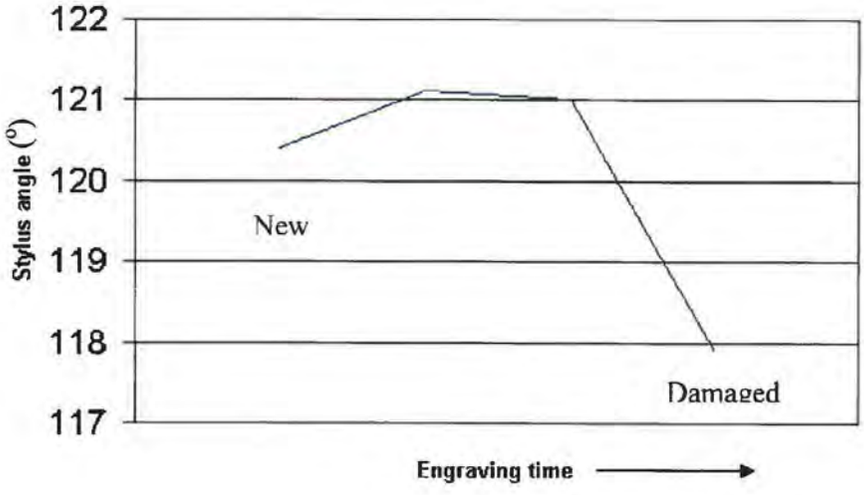

Graph A1.1 – Stylus angle change (120° stylus)

The wear of the diamond, although small, is clear, going from 120° to 118° over the engraving of a number of cylinders. Thus the angle changes significantly between new and the point at which it was damaged and repolished. It is not however, possible to draw trends from these results due to the spread of the data and uncertainty of the

timescale due to low confidence in the extent of engraving performed by this diamond.

A1.1.2 Tip Wear Calculation

Visual inspection also indicated that wear of the diamond was occurring at the tip, Figure A1.0-4. The position of four points, two on each side of the diamond was measured, thus allowing a 'theoretical tip' point to be calculated. The 'lowest' point of the diamond can also be measured, and the distance between this actual tip and the theoretical tip can be calculated using trigonometry, Figure A1.5.

5.9a – New tip

5.9b – Used tip

Figure A1.0-4 – Diamond tips

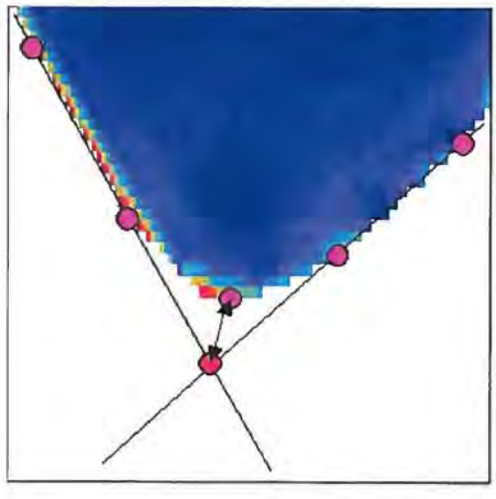

Figure A1.0-5 – Tip analysis

As shown in Graph A1.2 the wear at the diamond tip appears to be approximately linear and increases as the diamond is used for engraving.

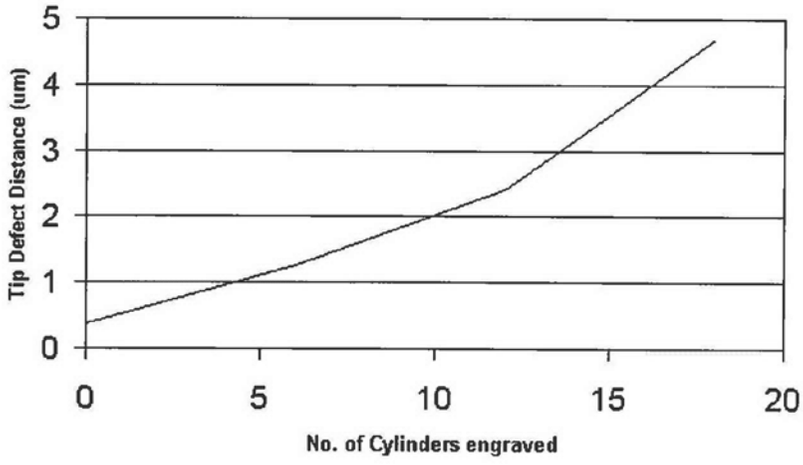

Graph A1.2 – Tip defect distance change with engraving time (120° diamond)

Although the wear appears to be small in extent, when considered against the cell depth in engraving, the change is significant. The combined effect of these two parameters is shown schematically in Figure A1.6.

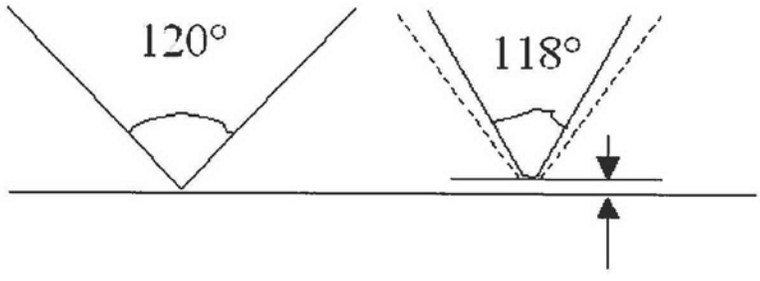

Figure A1.0-6 – Schematic of effects of worn diamond on cell volume. Exaggerated for clarity

A1.1.3 Summary of Diamond Measurements

It has been shown that the cutting surface of the diamond undergoes significant changes as a result of the engraving process. This was not initially recognised by the engravers, and so it is not possible to examine the shapes of the diamonds used while carrying out this investigation. It is however, recommended that further work is

carried out in this area to examine the effects of diamond variation, and in particular to monitor this more frequently in a systematic way over the working life of the diamond.

A2 Appendix 2 – Image Specifications

To the right is given details of the precise engraving specifications used in the production of the cylinder used for the ink release from image areas experiments.

The first column gives a reference number to each specification.

The second, third and fourth columns detail the engraving specifications

The fourth column details the arrays built into the image. The reference number is Array size, (in each case, L9), array number (1-5), row number within array (1-9).

The fifth column details nested arrays, and gives the additional array details for experiments which appear in multiple arrays

The sixth column details where in the image, this engraving is found. Reference is quadrant (a-e), column (as shown below)

	Cell (°)	Ruling (lpcm)	Stylus (°)	Array Ref.	Nested Reference	Location
1	37	60	130	9.1.1		ai
2	37	70	130	9.1.2	9.2.2	ae,ei
3	37	80	130	9.1.3		ah
4	45	60	130	9.1.4	9.3.2	ea
5	45	70	130	9.1.5	9.2.6, 9.3.8	ba,ca,da
6	45	80	130	9.1.6	9.3.8	am
7	57	60	130	9.1.7		bi
8	57	70	130	9.1.8	9.2.8	be,ce
9	57	80	130	9.1.9		bj
10	37	70	120	9.2.1		dl
11	37	70	140	9.2.3		df
12	45	70	120	9.2.4	9.3.2	dk
13	45	70	140	9.2.6	9.3.8	de
14	57	70	120	9.2.7		dj
15	57	70	140	9.2.9		dd
16	45	60	120	9.3.1		di
17	45	80	120	9.3.3		dh
18	45	60	140	9.3.7		dc
19	45	80	140	9.3.9		db
20	30	60	130	9.4.1		am
21	30	70	130	9.4.2		al
22	30	80	130	9.4.3		ak
23	40	60	130	9.4.4		aj
24	40	70	130	9.4.5		ai
25	40	80	130	9.4.6		ah
26	60	60	130	9.4.7		ag
27	60	70	130	9.4.8		af
28	60	80	130	9.4.9		ae
29	37	50	130	9.5.1		bi
30	37	90	130	9.5.2		bb
31	37	100	130	9.5.3		bg
32	45	50	130	9.5.4		bf
33	45	90	130	9.5.5		bh
34	45	100	130	9.5.6		bd
35	57	50	130	9.5.7		bc
36	57	90	130	9.5.8		be
37	57	100	130	9.5.9		cn
38	37	70	110	g		cg
39	45	70	110	h		ci
40	57	70	110	i		ck
41	30	70	110	e		cf
42	40	70	110	a		ch
43	60	70	110	f		cm
44	30	60	110	g		cd
45	40	60	110	h		ce
46	60	60	110	i		cj
47	51	60	130	j		cm
48	51	70	130	k		cl
49	51	80	130	l		ck
50	51	70	120	m		dg
51	51	70	140	n		da
52	45	70	130			bn
53	45	70	130			an
54	37	70	110			cj

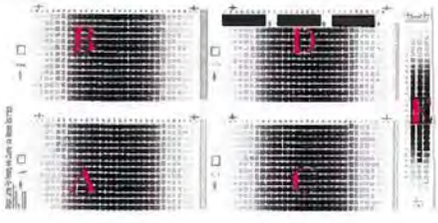

A3 Appendix 3 – Raw data example (cell volume analysis)

Below is shown a typical set of data for the analysis of an orthogonal array investigating compression ratio and screen ruling. The orthogonal array matrix is shown on the top left of the image, with matrixed results data to the right of this. Calculated results for each level are shown directly below the orthogonal array matrix, while processing of these results is carried out to the right of the results. Data is then graphed at the bottom.

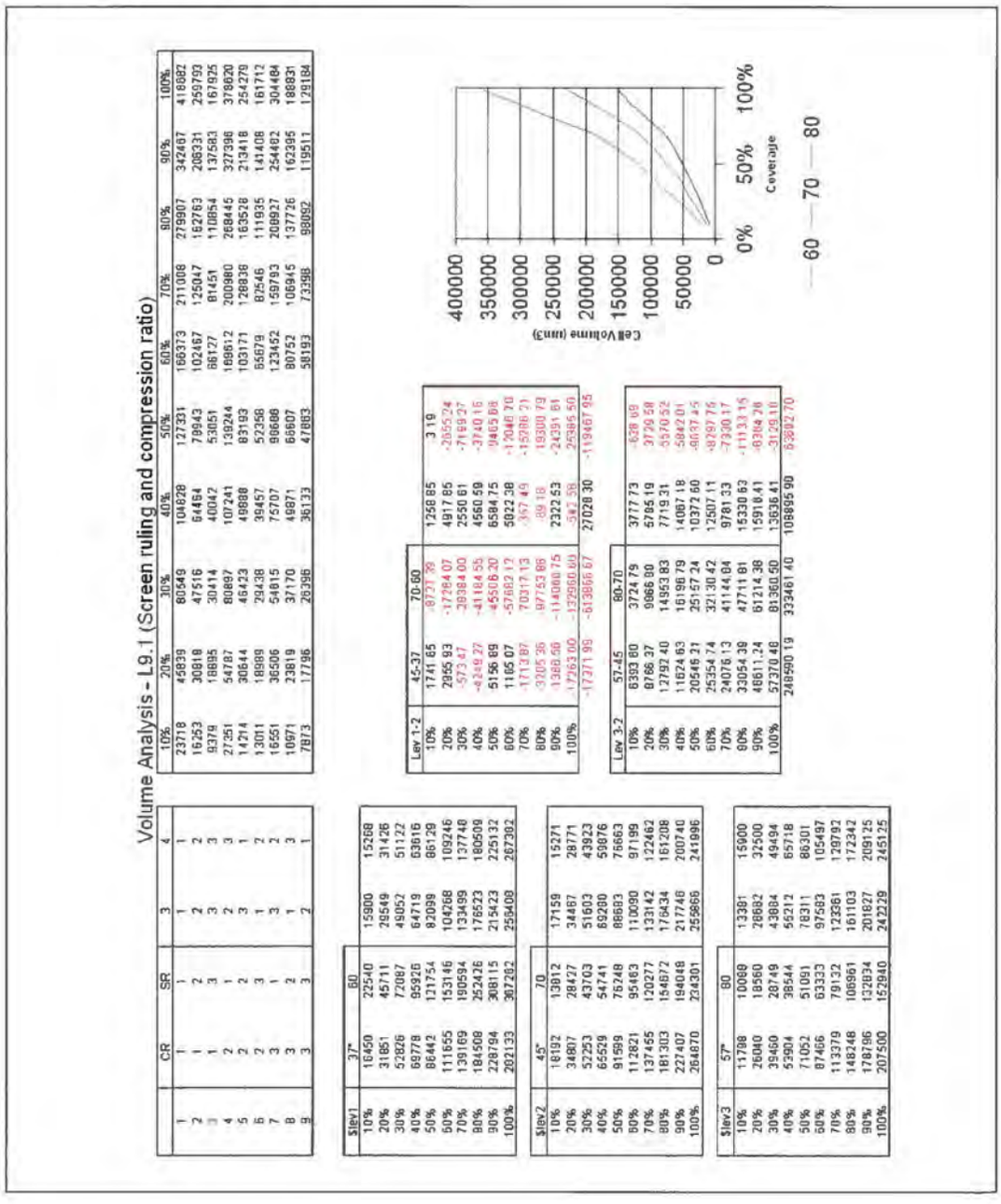

A4 Appendix 4 – List of publications and presentations

Publications and Reports

Bohan M.F.J., Korochkina T.V., Claypole T.C. and Gethin D.T. "*Analysis of Doctor Blade Loading and Wear*" 55th TAGA Technical Conference, 2003

Korochkina T.V., Bohan M.F.J., Clist A.M., Claypole T.C. and Gethin D.T. "*Monitoring and Measurement of Doctor Blade Load During the Scumming Trial at Teich Flexibles Ltd.*" WCPC 07/2002

Korochkina T.V., Bohan M.F.J., Clist A.M., Claypole T.C. and Gethin D.T. "*Monitoring and Measurement of Doctor Blade Load During the Scumming Trial at Printpack UK Ltd.*" WCPC 03/2002

Korochkina T.V., Bohan M.F.J., Clist A.M., Claypole T.C. and Gethin D.T. "*Monitoring and Measurement during the Process ParameterTrial at BASF*" 11/2001

Bohan M. F. J., Clist, A. M., Claypole, T. C. and Gethin, D. T. "*Characterisation of Gravure Cylinders*' TAGA 2001 pp1-12

Presentations.

Most of these were presented to the Rotogravure Printing Technology Group (RPTG) during the completion of this project.

Clist, A.M. and Bohan M.F.J. "*Interferometry of Printed Substrate*" Rotogravure Printing Technology Group, 13/3/2003

Clist, A.M. and Bohan M.F.J. "*Interferometric evaluation of engraving characteristics on cells and cell geometry*" RPTG, 13/3/2003

Bohan M.F.J. and Clist A.M. "*An Investigation into Engraving Diamond Wear*" RPTG 13/3/2003

Clist A.M. and Bohan M.F.J. "*Interferometric Evaluation of Engraving Characteristics on Cells and Cell Geometry*" RPTG 27/11/2002

Whittaker S.D. and Clist A.M. "*GCMS Analysis of Printed Substrate*" RPTG 27/11/2002

Clist A.M. and Bohan M.F.J. "*A Practical Investigation into Scumming*" RPTG 27/11/2002

Bohan M.F.J. and Clist A.M. "*An Investigation into Engraving Diamond Wear*" RPTG 27/11/2003

Clist A.M. and Bohan M.F.J. "*Interferometric Evaluation of Engraving Characteristics on Cells and Cell Geometry*" RPTG 8/10/2002

Clist A.M. and Bohan M.F.J. "*A Practical Investigation into Scumming*" RPTG 8/10/2002

Bohan M.F.J. and Clist A.M. "*An Investigation into Engraving Diamond Wear*" RPTG 8/10/2002

Clist A.M. and Bohan M.F.J. "*Measurement of Engraving Diamonds*" Institute of Physics, 10/2002

Bohan M.F.J. and Clist A.M. "*Interferometric Measurement of Gravure* Cells" Veeco Users Meeting, Huddersfield 12/09/2002

Clist A.M. and Bohan M.F.J. "*The Effects of Engraving Characteristics on Printed Density*" RPTG 5/3/2002

Whittaker, S.D. and Clist A.M. "*TD-GC-MS*" RPTG 5/3/2002

Bohan M.F.J. and Clist A.M. "*An Investigation into Engraving Diamond Wear*" RPTG 5/3/2002

Clist A.M. and Bohan M.F.J. "*A Practical Investigation into Scumming*" RPTG 9/10/2001

Clist A.M. and Bohan M.F.J. "*Cylinder Engraving Repeatability*" RPTG 9/10/2001

Bohan M.F.J. and Clist A.M. "*Measurement of Gravure Cells*" RPTG 26/06/2001

Clist A.M. and Bohan M.F.J. "*Cylinder Engraving Repeatability*" RPTG 26/06/2001

Korochkina T.V. and Bohan M.F.J. "*Doctor Blade Monitoring and Measurement*" RPTG 26/06/2001

Bohan M.F.J. and Clist A.M. "*Interferometric Measurement of Gravure Cells*" Veeco Users Meeting, London University, 26/03/2001

A5 – Appendix 5 – Glossary

CIE — Commission Internationale De L'Eclairage. The international commission on illumination. A body which defines standards in colour.

CIEL*a*b* — A colour space in which L^*, a^* and b^* are plotted at right angles to each other. 'L' defines the lightness of a sample, from 0 (black) to 100 (white), while 'a' defines the red-greenness of the sample, and 'b' defines the yellow-blueness of the sample. Colour difference (ΔE) is defined as the mathematical distance between two points. For further details see Hunt []. A representation of colour space is given in Figure 2.2.

Colour — Definition of a colour using a defined colour space. CIEL*a*b* space is used for all colour descriptions used within this thesis, D50 illuminant, 2° observer angle and a D65 filter.

Compression Ratio — Unlike the other volume, multicolour processes, it is not possible to produce cells at a variety of screen angles to prevent moiré, and as such it is necessary to utilise another technique. This is shown schematically below. It is controlled by controlling the speed of rotation and the speed of vibration of the engraving diamond. The effects are shown below, figure A5-1

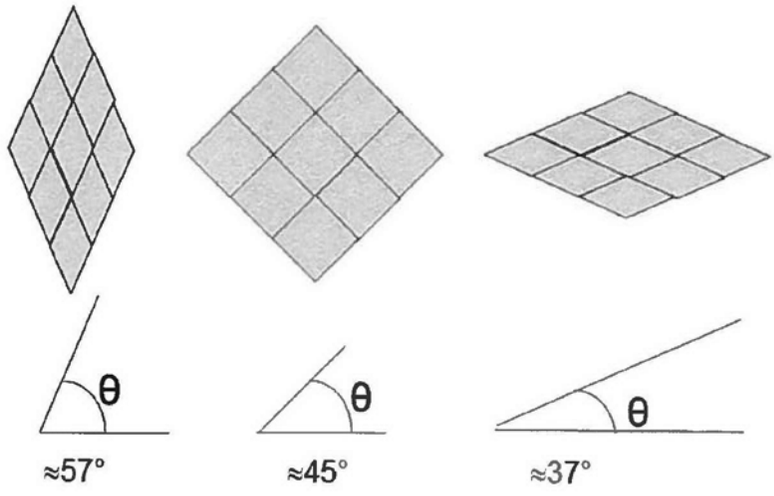

Figure A5-1 Schematic of Compression Ratio

Delta E (ΔE) The mathematical difference between two points in CIEL*a*b* colour space, defined as the colour difference between two colours. Equal Delta E's equate to perceptually equal colour differences

Density Logarithm of the reciprocal of the reflectance. A higher density indicates a stronger colour. Only used on process colours (cyan, magenta, yellow, black). Using ANSI T,

Line Ruling As screen ruling

Moiré Optical interference patterns cause by slight misalignment of dots when overlaid to create a multicolour image. By separating the screen angles / compression ratios as much as possible, moiré is minimised. Examples are shown below, figure A5-2

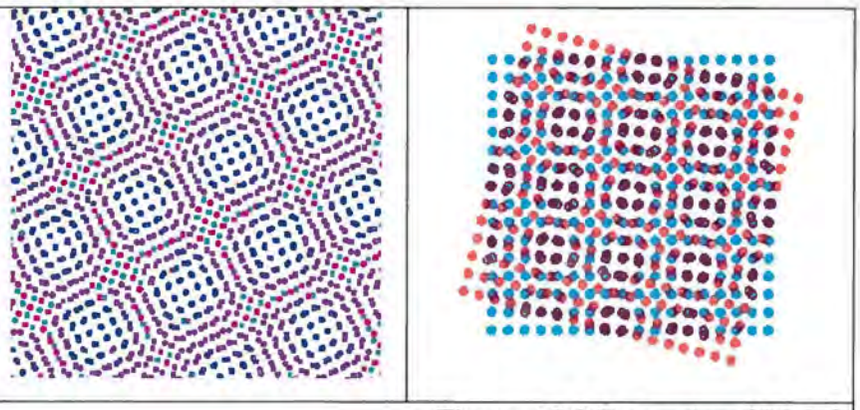

Figure A5-2 Examples of Moiré

R_a The average height deviation from a mean height (Z=height, N and M are the number of data points in each direction of the array in a 3D R_a measurement)

$$R_a = \frac{1}{MN}\sum_{k=1}^{M}\sum_{j=1}^{N}\left|Z_{jk}\right|$$

R_{ku} The kurtosis of the sample is a measure of the 'spikiness' of a sample. It is very sensitive to outlying values.

$$R_{ku} = \frac{1}{R_q^4}\cdot\frac{1}{N}\sum_{j=1}^{N}Z_j^4$$

R_p Maximum peak height

R_q Root mean squared average of height deviation within the measurement area, measured from the mean height

$$R_q = \sqrt{\frac{1}{MN}\sum_{k=1}^{M}\sum_{j=1}^{N}\left|Z_{jk}^2\right|}$$

R_{sk} The 'skew' of the sample is a measure of the asymmetry of the profile around the mean line

$$R_{sk} = \frac{1}{R_q^3}\cdot\frac{1}{N}\sum_{j=1}^{N}Z_j^3$$

R_t The vertical distance from the highest peak on the sample to the lowest trough

$$R_t = R_p + R_v$$

R_v Maximum valley depth

R_z The vertical distance between the average of the five highest points to the average of the five lowest points in the sample

$$R_z = \frac{1}{N}[(H_1 + H_2 + ...H_n) - (L_1 + L_2 + ...L_n)]$$

Reflectance The ratio of reflected light to the incident light

Screen Ruling The number of lines of engraved cells in a given distance. All examples used in this thesis are given in lpcm – lines per cm, ie, the number of cells in one linear cm. Examples of a picture using a fine screen (high lpcm - left) and a coarse screen (low lpcm – right) are shown below.

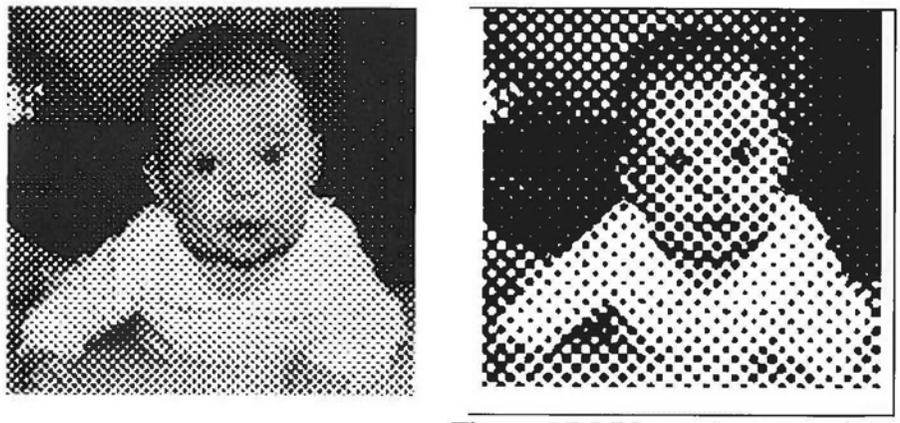

Figure A5-3 Line ruling examples

Stylus angle The angle of the tip of the cutting face of an engraving diamond.

A6 – Appendix 6 – Statement of Confidence

Errors exist in all measurements, and it is necessary to measure a suitable number of samples in order to calculate a suitable average value to have the desired accuracy and reliability to allow conclusions to be drawn from them. As the most variable data examined, the example of printed dot volumes will be examined in more detail.

According to central limit theorem [68], if random samples, size n are taken from a distribution with mean, μ and standard deviation σ, the sampling distribution of $\overline{x}$ will be approximately normal with mean μ and standard deviation $\sigma/n^{0.5}$, the approximation improving as n increases.

If examining the size of printed dots, the volume was measured using the method detailed in chapter 3, results being as follows;

3245	3149	2542	2356	2589
3903	3027	2732	2502	3072
2648	2597	2639	2439	2943
2714	2783	2657	2250	2496

Figure A6-1 Volumes of dots (μm^3)

Thus $n = 20$

$\sigma = 377.1 \mu m^3$

$\mu = 2764.15 \mu m^3$

According to the manufacturers of the white light interferometer, the errors in measurement should be less than $\pm 40 \mu m^3$.

Thus the probability of the sample mean being outside the mean $\pm 40 \mu m^3$ is dependent on the sample size, n.

From central limit theorem, the sampling distribution of $\overline{x}$ is normal, with the same mean ($2764.15 \mu m^3$), but with a standard deviation equal to $377.1/20^{0.5} = 84.3 \mu m^3$

Given that the variation between dot sizes at different screen rulings, compression ratios etc. is between 100μm and 1000μm, selecting a minimum variation of 50μm as indicating an actual change, rather than a measurement error, investigating the probability of a sample mean exceeding the mean±50μm^3 indicates the probability that the change observed is an actual change, rather than a measurement error.

If the probability of sample means exceeding the mean ±50μm^3 is calculated using a variety of values for *n*, the following relationship is found.

N	sd of xbar	Table Val
1	84.32	0.59
2	59.63	0.84
3	48.68	1.03
4	42.16	1.19
5	37.71	1.33
6	34.42	1.45
7	31.87	1.57
8	29.81	1.68
9	28.11	1.78
10	26.67	1.88
11	25.42	1.97
12	24.34	2.05
13	23.39	2.14
14	22.54	2.22
15	21.77	2.30
16	21.08	2.37
17	20.45	2.44
18	19.88	2.52
19	19.35	2.58
20	18.86	2.65

Figure A6-2 – Probability calculations

Using this example, and reading the probability from a standard table of areas under the normal curve (for example, table 1, appendix B in [68]), using 12 samples gives 97.98% probability that the variation is caused by process change, and rather than measurement errors.

Since measurements indicate the changes caused to printed dot volumes between screen rulings, stylus angles and compression ratios are of the order of $100\mu m^3$ to $1000\mu m^3$ recalculating for probability, it is 99.999% likely to be due to observed size differences rather than measurement errors at $100\mu m^3$ and 99.9999% likely at $1000\mu m^3$.

A6.1 Total error in ink release calculation

The total error in a measurement is the summation of all the errors involved in the measurement. In the case of ink release, the measurement consists of three parts at which errors are combined :

Calculation of Cell volume	0.15% (50% cell)
Calculation of Printed Volume	0.1% (50% dot)
Calculation of retained solvents	0.1%

Thus the total error in the measurements should be 0.15 + 0.1 + 0.1% = 0.35% and is thus insignificant compares with the values observed.